Conformational analysis of a cyclic AKH neuropeptide analog that elicits selective activity on locust versus honeybee receptor

Ibrahim A. Abdulganiyyu[a], Krzysztof Kaczmarek[c,d], Janusz Zabrocki [c,d], Ronald J. Nachman[c*], Elisabeth Marchal[e], Sam Schellens[e], Heleen Verlinden[e], Jozef Vanden Broeck[e], Heather Marco[b] and Graham E. Jackson[a**]

[a]Department of Chemistry and [b]Biological Sciences, University of Cape Town, Private Bag, Rondebosch, Cape Town, 7701, South Africa. [c]Insect Control and Cotton Disease Research Unit, Southern Plains Agricultural Research Center, U.S. Department of Agriculture, 2881 F/B Road, College Station, TX 77845 USA; [d]Lodz University of Technology, 90-924 Lodz, Poland; [e]Molecular Developmental Physiology and Signal Transduction, KU Leuven, Naamsestraat 59, 3000 Leuven, Belgium.

[*]Communicating Author, ron.nachman@usda.gov

[**]Communicating Author, graham.jackson@uct.ac.za

Keywords: conformational restriction, agonist, insect control, NMR, molecular dynamics

Abstract

Neuropeptides belonging to the adipokinetic hormone (AKH) family elicit metabolic effects as their main function in insects, by mobilizing trehalose, diacylgycerol, or proline, which are released from the fat body into the hemolymph as energy sources for muscle contraction required for energy-intensive processes, such as locomotion. One of the AKHs produced in locusts is a decapeptide, Locmi-AKH-I (pELNFTPNWGT-NH_2). A head-to-tail cyclic, octapeptide analog of Locmi-AKH-I, *cyclo*AKH (*cyclo*[LNFTPNWG]) was synthesized to severely restrict the conformational freedom of the AKH structure. *In vitro*, *cyclo*AKH selectively retains full efficacy on a pest insect (desert locust) AKH receptor, while showing little or no activation of the AKH receptor of a beneficial insect (honeybee). Molecular dynamic analysis incorporating NMR data indicate that *cyclo*AKH preferentially adopts a type II β-turn under micelle conditions, whereas its linear counterpart and natural AKH adopts a type VI β-turn under similar conditions. *Cyclo*AKH, linear LNFTPNWG-NH_2, and Locmi-AKH-I feature the same binding site during docking simulations with the desert locust AKH receptor (Schgr-AKHR), but differ in the details of the ligand/receptor interactions. However, *cyclo*AKH failed to enter the binding pocket of the honeybee receptor 3D model during docking simulations. Since the locust AKH receptor has a greater tolerance than the honeybee receptor for the cyclic conformational constraint in *in vitro* receptor assays, it could suggest a greater tolerance for a shift in the direction of the type II β turn exhibited by *cyclo*AKH from the type IV β turn of the linear octapeptide and the native locust decapeptide AKH. Selectivity in biostable mimetic analogs could potentially be enhanced by incorporating conformational constraints that emphasize this shift. Biostable mimetic analogs of AKH offer the potential of selectively disrupting AKH-regulated processes, leading to novel, environmentally benign control strategies for pest insect populations.

1. Introduction

Neuropeptides play an important role in the regulation of most critical metabolic, reproductive, developmental, and behavioural processes in the life cycle of insects. Therefore, neuropeptides and

61 their G-protein-coupled receptors are considered suitable targets for new insect control agents,
62 analogous to the rationale followed in the development of drugs for treatment of human disease
63 (Audsley & Down, 2015;Verlinden et al., 2014, Nachman, 2009a, Nachman et al., 2014a,b;
64 Nachman & Pietrantonio, 2010). Unfortunately, neuropeptides themselves generally fail to show
65 efficacy as insect control agents due to their susceptibility to peptidases in the gut and hemolymph
66 and, for the most part, an inability to efficiently penetrate the cuticle of an insect pest. However,
67 development of mimetic agonist or antagonist analogs that feature both enhanced biostability to
68 peptidases and bioavailability characteristics can lead to the disruption of the critical life processes
69 that neuropeptides regulate. Another important aspect of this research is the development of mimetic
70 neuropeptide analogs that are selective in their activity, negatively affecting the targeted pest species
71 without harm to beneficial insect species like the honeybee.

72 One family of neuropeptides, viz. the red pigment-concentrating hormone/adipokinetic hormone
73 (RPCH/AKH) family, is present in all insect orders investigated to date, and regulates intermediate
74 metabolism in insects (Gäde, 1990, 2003, 2004, 2009, Beenakkers et al., 1985). The potential of AKHs
75 as leads for development of novel pest control strategies has been previously discussed (Gäde &
76 Goldsworthy, 2003; Gäde, Šimek & Marco, 2017). The AKHs are synthesized in neurosecretory cells
77 of the corpora cardiaca (CC) and are chiefly known for their action to mobilize stored fuels (glycogen
78 or triacylgycerols) from the fat body; the resulting trehalose, diacylgycerol, or proline are released into
79 circulation for metabolism (Gäde, 2004). Diacylglycerols, for instance, can then be used by insects for
80 immediate contraction of muscles during locomotory events (reviewed by Lorenz and Gäde, 2009).
81 AKH peptides are structurally characterized as being short peptides of between eight and 10 amino
82 acid residues, with posttranslational modifications at the N-terminus (a pyroglutamate residue) and the
83 C-terminus (amidation); at position 2 from the N-terminus can be the aliphatic amino acids leucine,
84 isoleucine or valine, or the aromatic phenylalanine or tyrosine; threonine or asparagine are always at
85 position 3, the aromatic amino acids phenylalanine or tyrosine at position 4, the branched amino acids

serine or threonine at position 5, and always the aromatic tryptophan and the simple glycine at positions 8 and 9, respectively; whereas at positions 6,7, and 10 a large variety of amino acids can be employed (Gäde, 2009; Gäde & Marco, 2006, 2013; Marco & Gade, 2015).

GPCRs for AKHs in insects are known since 2002 to have seven membrane-spanning domains, and to belong to the rhodopsin class of receptors (Staubli *et al.*; 2002; Park *et al.*, 2002); although the AKH receptors are specific for AKH peptides, there may be cross-activation from interspecific AKHs (see for example, Marco *et al.*, 2013; Marchal *et al.*, 2018). It is, therefore imperative that any lead AKH analog for future pesticide design should be tested for receptor specificity. Head-to-tail cyclic (Nachman *et al.*, 1991; Roberts *et al.*, 1997; and Zhang *et al.*, 2009), and other restricted-conformation (Nachman *et al.*, 1998, 2002, 2009a, 2009b, 2009c, 2010, 2013, 2014; Kaczmarek et al., 2007; Moyna et al., 1999a, 1999b; Taneja-Bageshwar *et al.*, 2008; Zhang *et al.*, 2011) analogs of insect neuropeptides have been synthesized and tested in bioassays to study their active conformations. In the current study, we have designed and synthesized a head-to-tail cyclic, octapeptide AKH analog to severely restrict the conformations available to an AKH neuropeptide sequence. The *cyclo*AKH demonstrates selectivity in that it retains full efficacy on a locust AKH receptor, while showing little or no activation of a honeybee AKH receptor. The conformation of the *cyclo*AKH and its linear equivalent are also investigated in the current study in order to identify conformational characteristics that potentially influence interaction with the locust receptor and, specifically its selective activation. Such information can aid in the development of mimetic agonistic and/or antagonistic AKH analogs that feature selective, environmentally-friendly pest management capabilities.

2. Materials and Methods

2.1 *Analog synthesis and purification*:

The synthesis of the linear peptide precursor of the cyclic peptide and the linear analog [Oic]Locmi-AKH-I, was performed on an ABI 433A Peptide Synthesizer in the scale of 0.25 mmole according to Fmoc/HBTU/DIPEA methodology on Rink-Amide resin (Taneja-Bageshwar et al., 2009). The cyclic-

AKH analog, *cyclo*AKH, contains two residues, one Gly and one Pro, which are not prone to epimerization during activation. Either one could be placed at the C-terminus of the linear precursor targeted for cyclization. We used glycine attached to 2-chlorotityl resin, obtaining H-Leu-Asn(Trt)-Phe-Thr(t-Bu)-Pro-Asn(Trt)-Trp(Boc)-Gly-2Cl-Trityl resin. This type of resin allows for the final cleavage of the peptide with all protecting groups at side chains untouched (Trt, t-Bu, Trt, and Boc, consecutively). Peptide head-to-tail cyclization requires high dilution to avoid inter-molecular reaction. We performed cyclization in DCM at a concentration of <0.5mmol/1L with the aid of 3 equivalents of EDC in the presence of HOAt. and the reaction was checked for completion on RP-HPLC. After concentration to about one/fourth of the original volume, the DCM solution was extracted 3 times with 0.1N HCl aq. and 1M sodium bicarbonate solution and then concentrated to dryness. The residues were treated with a cocktail composed of TFA/DMB/TIS (92.5:5:2.5) for deprotection of side chains and then the product was precipitated with ether.

The cyclic analog and linear [Oic]Locmi-AKH-I were desalted on a Waters C_{18} Sep Pak cartridge (Milford, MA) in preparation for purification by HPLC. The analog was purified on a Waters Delta-Pak C_{18} reverse-phase column (8 x 100 mm, 15 µm particle size, 100 Å pore size) with a Waters 510 HPLC system with detection at 214 nm at ambient temperature. Solvent A = 0.1% aqueous trifluoroacetic acid (TFA); Solvent B = 80% aqueous acetonitrile containing 0.1% TFA. Initial conditions were 10% B followed by a linear increase to 90 % B over 40 min.; flow rate, 2 ml/min. Delta-Pak C_{18} retention times: *cyclo*AKH (*cyclo*[LNFTPNWG]): 6.2 min; pQLNFT**[Oic]**NWGT-NH_2: 4.5 min; The analogs were further purified on a Waters Protein Pak I 125 column (7.8 x 300 mm). Conditions: isocratic using 80% acetonitrile containing 0.1% TFA; flow rate, 2 ml/min. Waters Protein Pak retention times: *cyclo*AKH (*cyclo*[LNFTPNWG]): 6.0 min; pQLNFT**[Oic]**NWGT-NH_2: 6.25 min. Amino acid analysis was carried out under previously reported conditions (Nachman et al., 1991) to quantify the analogs and to confirm identity: *cyclo*AKH (*cyclo*[LNFTPNWG]): F[1.0], G[0.9], L[1.0], N[1.7], P[0.9], T[1.0]; pQLNFT**[Oic]**NWGT-NH_2: E[1.0], G[1.0], L[0.9], N[1.7],

T[1.7]. The identity of the analogs was also confirmed by MALDI-MS on a Kratos Kompact Probe MALDI-MS instrument (Shimadzu, Columbia, Maryland). The following molecular ions (MH^+) were observed: *cyclo*AKH (*cyclo*[LNFTPNWG]): 931.6 (calc.931.3 [MH^+]); pQLNFT**[Oic]**NWGT-NH_2: 1213.2 (calc 1213.2 [MH^+]).

2.2 *In vitro calcium reporter assay for SchgrAKHR and ApimeAKHR:*

The molecular cloning of the *Schgr*AKHR and the *Apime*AKHR was described by Marchal *et al.* (2018). In short, RNA was extracted from adult whole animal *A. mellifera* and from adult *S. gregaria* fat body using the RNeasy Lipid Tissue Kit (Qiagen, Germany) and reverse transcribed using the Transcriptor High Fidelity cDNA Synthesis Kit (Roche, Switzerland) as per manufacturer's recommendation. The resulting cDNA was used as PCR template in amplifying the adipokinetic hormone receptor transcripts of the specified insects using Q5 polymerase (New England Biolabs). The following primers were used in the PCR mix:

*Apime*AKHRF: *CACC*ATGGAAGTGATGGATTCTGACGCC,

*Apime*AKHRR: GTTAGTTCACAAATTGTACCAGATTACC;

*Schgr*AKHRF: *CACC*ATGGCGGGCCTCGAATCGG,

*Schgr*AKHRR: TCACCTTGCCTCCGTTGTTCTG.

'CACC' was added to the 5' end of each forward primer to obtain a kozak sequence necessary for efficient expression in vertebrate cell lines. The resulting PCR product was purified using the GenElute™ PCR Clean-Up Kit (Sigma-Aldrich, USA), cloned into pcDNA3.1/V5-His-Topo directional expression vector and transformed to One Shot® TOPO10 chemical competent *Escherichia coli* cells according to the manufacturer's guidelines (Invitrogen, Carlsbad, CA, USA). The cells were grown overnight at 37 °C on Luria Bertani (LB) agar plates (35 g/L; Sigma-Aldrich) containing 10 mg/mL ampicillin (Invitrogen). We transferred grown colonies to 5 mL LB medium (with 10 mg/mL ampicillin; Sigma-Aldrich). After growing overnight at 37 °C, the receptor DNA containing vector

was purified using 'GenElute™ HP Plasmid Miniprep' kit (Sigma-Aldrich) and sequenced using the ABI PRISM 3130 Genetic Analyzer (Applied Biosystems, USA). Colonies containing the correct vector were used to inoculate 100 mL LB medium with 10 mg/mL ampicillin and were grown overnight at 37 °C in a shaking incubator. We purified the plasmids using the 'GenElute™ Plasmid Maxiprep Kit' (Sigma-Aldrich).

The activity of the two AKH receptors was analyzed in an *in vitro* calcium reporter assay using CHO-WTA11 cells, which contain a promiscuous Gα16 subunit that will induce an intracellular Ca^{2+}-increase upon receptor activation independent of the natural signaling cascade (Offermanns & Simon, 1995; Stables *et al*., 1997). Cell culture and transfection were performed as described by Marchal & Schellens *et al*. (2018). We cultured the cells at 37 °C with constant supply of 5% CO_2 in Dulbecco's Modified Eagle's Medium Nutrient Mixture F-12 Ham (DMEM/F12) with l-glutamine, 15 mM HEPES, sodium bicarbonate and phenol red (Sigma-Aldrich) enriched with 10% heat-inactivated fetal bovine serum (Gibco), 100 IU/mL penicillin and 100 µg/mL streptomycin (Gibco) and 250 mg/mL Zeocin (Gibco).

For transfection of the cells (T75 flasks at 60–80% confluency), we dissolved 5 µg pcDNA3.1-receptor or empty pcDNA3.1 vector in 2.5 mL Opti-MEM® (Gibco) supplemented with 12.5 µL Plus™ Reagent of the Lipofectamine LTX Kit (Invitrogen) in 5 mL polystyrene round-bottom tubes. We incubated this mixture for 5 min at room temperature. Thereafter, we added 30 µL LTX and incubated this mixture again at room temperature for 30 min. We then removed the cell medium and added the transfection mixture dropwise followed by 3 mL fresh complete culture medium. After an overnight incubation at 37 °C with constant supply of 5% CO_2, we added 10 ml of complete culture medium and allowed the cells to grow for another night (37 °C, 5% CO_2). Ligand-induced changes in intracellular Ca^{2+} in the cells were analyzed in a calcium reporter assay as described by Marchal & Schellens *et al*. (2018). An endogenous ligand for both receptors (pQLNFSTGWamide=Schgr-AKH-II = *Apime*-AKH), *Locmi*-AKH-I (pQLNFTPNWGTamide = *Schgr*-AKH-I), a linear analog of Locmi-AKH-I

(pQLNFT[Oic]NWGTa) and a cyclic analog, *cyclo*AKH, were tested at different concentrations. pQLNFSTGWamide and Locmi-AKH-I were custom-synthesized by Synpeptide Co. (Shanghai, China) and CPC Scientific, Inc. (San Jose, CA), respectively. The transfected cells were detached using phosphate buffered saline (PBS), supplemented with 0.2% EDTA, and rinsed off the flask using DMEM/F12 with l-glutamine and 15 mM HEPES (Sigma-Aldrich). The number of viable cells was determined using the TC20 automated Cell Counter (Bio-Rad, Hercules, CA, USA). In order to achieve a cell density of 5×10^6 cells/mL, we centrifuged the cells for 5 min at 800 rpm and resuspended them in the appropriate volume of sterile filtered bovine serum albumin (BSA) medium (DMEM/F12 with l-glutamine and 15 mM HEPES, complemented with 0.1% BSA). In addition, we loaded the cells with 5 µM Coelenterazine h (Invitrogen) by gently shaking them at room temperature for 4 h in the dark to reconstitute the holo-enzyme aequorin. Before exposure to potential ligands dissolved in BSA medium, we diluted the cells tenfold in the same medium 30 min prior to the measurement. Thereafter, the Mithras LB 940 (Berthold Technologies, Bad Wildbad, Germany) injected 50 µL of the cells into every well (25,000 cells/well) of a 96-well plate. The machine measured the ligand-induced calcium response for 30 s, where after it added 50 µL of 0.1% Triton X-100 in order to measure the total cellular Ca^{2+}-response. The ligand-specific response was normalized using the total response (ligand + Triton X-100), which is directly related to the number of cells present in the well. A negative control (only BSA) was included in each row to correct the cell response of each well of the same row. We performed the calculations using the output file from the MicroWin software (Berthold Technologies) in Excel (Microsoft). Further analysis was done in GraphPad Prism 6.

2.3 *NMR measurements*

*Cyclo*AKH (335 nmole) was dissolved in 0.5 ml of 20 mM phosphate buffer (pH 5.0) with 10% (v/v) D_2O. An internal standard of 1% sodium 4,4-dimethyl-4-silapentane-1-sulfonate (DSS) was added. Linear-[LNFTPNWG-NH_2] was supplied by Pepmic Co. Ltd, China; the peptide purity was checked with HPLC–MS and found to be > 98% pure. Linear-[LNFTPNWG-NH_2] peptide was readily soluble

in 30% DMSO and a dodecylphosphocholin (DPC) micelle solution. 1 mg of sample was dissolved in 0.5 ml of either 20 mM phosphate buffer + 30%DMSO or 10:1 (v/v) H2O: D_2O solution, which was 150 mM in deuterated DPC-d38(Cambridge Isotopes, 98.6% d) and buffered at pH 4.5 with 20 mM potassium phosphate buffer. An internal standard of 1% sodium 4,4-dimethyl-4-silapentane-1-sulfonate (DSS) was added. Peptide–peptide interactions were minimized by maintaining a peptide to micelle ratio of 1:3 with 50 molecules of DPC per micelle.

NMR experiments on linear-[LNFTPNWG-NH_2] were conducted on a Bruker Avance 600 MHz spectrometer, while a Bruker 800 MHz spectrometer with cryoprobe was used for *cyclo*AKH. Spectra were recorded with excitation sculpting for water suppression using the dipsi2esgpph pulse, sequence, (mixing time, 60 or 80 ms) for Total Correlation Spectroscopy (TOCSY), and noesyesgpph for nuclear Overhauser effect spectroscopy (NOESY)(mixing time, 150 or 300 ms)(Braunsch Weiler & Ernst, 1983; Jeener et al., 1979). Spectral assignments were according to the method of Wüthrich (Weber et al., 1988; Wüthrich, 1986) . Heteronuclear Single Quantum Coherence (HSQC) spectra (Sklenar *et al*., 1993; Sklenar & Bax, 1987) were used for the ^{13}C and ^{15}N assignments. The diffusion coefficients were measured using the DOSY pulse sequence, ledbpgppr2s, a p30 (small delta) of 3ms and a d20 (big delta) of 0.1 s. Inter-proton distances from the 2D NOESY cross-peak intensities were calculated using the isolated spin pair approximation (ISPA) (Thomas *et al*., 1991):

$$r_{ij} = r_{ref}(a_{ref}/a_{ij})^{1/6}$$

Where r_{ij} is the inter-proton distances and a_{ij} is the 2D nOe cross peak intensity between protons *i* and *j*. ISPA was used as a suitable approximation since a short mixing time of 150 ms was used in the NOESY experiment. Hence, the effects of spin diffusion were small (Stone *et al*., 2007a,b). Since nOe measurements are biased towards short inter-nuclear distances lower and upper error limits were achieved by adding 10% and 20% to each of the measured distances respectively (Jackson *et al*., 2009). The germinal Pro^5 H_β protons served as the reference, a_{ref}, with a set inter-nuclear distance of 0.18 nm.

2.4 *Peptide molecular dynamics*

The starting structures for the conformational search of both the conformationally-restrained *cyclo*AKH and linear-[LNFTPNWG-NH_2] were built using Insight II 2005 and energy minimized for 50,000 steps using the steepest descent algorithm. NMR distance restrained molecular dynamics simulations in a vacuum, water and DPC were achieved using GROMACS version 5.0 (Abraham *et al.*, 2015; Van Der Spoel *et al*., 2005). All simulations were performed using the OPLS-AA/L all–atom force field and constant temperature, pressure and number of particles (NPT). The LINCS algorithm was used to constraint all bonds. Because of the strained nature of the cyclic peptide it was necessary to use a time step of 1 fs to avoid warnings from the LINCS algorithm. For the restrained simulations, time-averaged NMR restraints with a disre-tau of 10 ps, a time step of 2 fs were used. A square well restraints potential was used where the potential was set to zero between the lower and upper bounds and increased quadratically (force constant1000 kJ $mol^{-1}nm^{-1}$) beyond that. The LINCS algorithm was applied to constrain all bonds. A cut-off of 1.0 nm was used for van der Waals and electrostatic interactions for real space calculations. Vacuum simulations were first performed to search conformational space by collecting 100 snapshots of the trajectory during a 10 ns simulation at 600 K. Each conformation was then annealed to 300 K over 50 ps. Cluster analysis of the resulting structures, exploiting the linkage algorithm of GROMACS and a cut-off of 0.1 nm on the backbone atoms, gave a single large cluster. The conformer with the lowest energy in the cluster was used for simulations in water. Using the single point charge water model or TIP4P water model, a box containing the peptide, chloride to neutralize any charge and 7000 water molecules was constructed. Following equilibration, molecular dynamics was performed for 10 ns at 300 K under NVT conditions. In total, 200 structures were collected at 50 ps intervals. Cluster analysis was then done as before, and the results used in the DPC/water simulations. For simulations in a water/DPC mixture, the lowest energy structure from the simulations in water was placed in the center of a 7 nm cubic box filled with approximately 10 000 water molecules and a 50 DPC molecule, micelle (Tieleman, van der Spoel, &

Berendsen, 2000). The micelle was translated so that the center of the micelle was at the bottom edge of the box. This meant that, using periodic boundary conditions, half the micelle was at the bottom of the box and the other half was at the top. The peptide was then placed in the center of the box. Energy minimization was carried out using the steepest descent method for 10,000 steps to a tolerance of 10 kJ mol^{-1}or to machine precision. Two stages of system equilibration were performed to solvate the peptide and to accomplish a steady state of temperature, pressure, and density. The first stage of equilibration involved performing molecular dynamics (MD) for 100 ps under NVT conditions at 300K followed by a second stage under NPT conditions. The final MD simulation was for 10 ns during which 200 structures were collected. Cluster analysis was performed in the same manner as before.

2.5 *Construction of Apime*-AKHR model

The primary sequence of *Apime*-AKHR Genbank sequence (AY898652) (Yang et al., 2018), was utilized to elucidate the 3D structure of the AKH-receptor. PSIPRED 4.0 and MEMSAT-SVM programs available on http://bioinf.cs.ucl.ac.uk/web_servers/ were used to predict the secondary structure and the transmembrane regions of the receptor. PSIPRED 4.0 makes use of two feed-forward neural networks, which perform analysis on output obtained from PSI_BLAST (Altschul et al. 1990; McGuffin et al., 2000) same as the MEMSAT-SVM programs (Jones, 2007).

The conserved amino acid residues of *Apime*-AKHR are consistent with it belonging to the class A GPCR family. The PSI_BLAST search tool was used to select the best template structure for use as the target template. The crystal structure of the Apelin receptor (5VBL.1B) (Ma et al., 2017) available in the Protein Data Bank (Berman et al., 2014) was selected. This crystal structure was used as the target template for sequence alignments of *Apime*-AKHR using Clustalw2 available at https://www.ebi.ac.uk/Tools/msa/clustalw2. The GMQE (Global Model Quality Estimation) was used for quality estimation.

Upon achieving a suitable alignment, homology modelling was conducted using the SWISS-MODEL server, a web-based service strictly dedicated to protein structure homology modelling (Guex et al., 2009). The model was built based on the target-template alignment using ProMod3 installed in the SWISS-MODEL server. Coordinates conserved between the target and the template were copied from the template to the model. Insertions and deletions were remodeled using the SMTL (version 28/2/2019, PDB release 22/2/2019) fragment library. After the sidechains were rebuilt, the resulting model was optimized using an opls force field. Loop modelling was done with ProMod3 alongside PROMOD-II as an alternative model. The model was viewed and analyzed using the program PYMOL (Schrödinger, 2010).

2.6 *Docking studies*

The Protein Preparation Wizard and LigPrep of the Schrödinger suite of programs (Schrödinger Inc., New York, NY, USA) were used to prepare the receptors, Schgr-AKHR (from Jackson *et al.*, 2019) and *Apime*-AKHR, and peptides for docking simulations. The lowest energy structure of *cyclo*AKH and Linear-[LNFTPNWG-NH_2] from the DPC micelle solution simulations were used. *Glide* docking (version 2019-3, Schrodinger, LLC, New York, NY, 2019) was used for peptide docking with a grid space of 72 x 72 x 72, which covered all extracellular loops and helices. The receptor grid was generated for peptide ligands and the docking precision was SP-Peptides. This setting automatically increases the number of poses collected.

3. Results and discussion

3.1 In vitro calcium reporter assay for SchgrAKHR and ApimeAKHR:

The dose-dependent activity of the Schgr-AKH-II (pQLNFSTGWa) and Locmi-AKH-I (pQLNFTPNWGTa) were compared on the desert locust *Schistocerca gregaria* and honeybee *Apis melifera* AKH receptors in Figure 1A. The dose-dependent activity of Schgr-AKH-II (pQLNFSTGWa) and two *Locmi*-AKH analogs, viz. [Oic^5]Locmi-AKH-I (pQLNFT[Oic]NWGTa)

and *cyclo*AKH (*cyclo*[LNFTPNWG]), were compared on the desert locust *Schistocerca gregaria* and honeybee *Apis melifera* AKH receptors in a separate trial. Schgr-AKH-II is native to both the desert locust and the honeybee, and the peptide showed a very similar activity on the cell lines expressing the locust (EC_{50} = 1.04 x 10^{-9}M) and honeybee receptor (1.28 x 10^{-9}M) (Figure 1). *Locmi*-AKH-I is a native decapeptide of the desert locust. The cyclic AKH analog of the current study is designed after the *Locmi*-AKH-I sequence. Locmi-AKH-I and a Locmi-AKH-I analog in which Pro^5 is replaced with the Pro analog octahydroindole-2-carboxylic acid (Oic) were evaluated on the two AKH receptor cell systems in separate trials in the current study. The unmodified Locmi-AKH-I was tested and found to match the activity of Schgr-AKH-II on the locust receptor (EC_{50} - 2.22 x 10^{-9} M) and a somewhat lower activity (EC_{50} – 7.62 x 10^{-8} M) on the honeybee receptor (Fig. 1A). Analog [Oic^5]Locmi-AKH-I (pQLNFT[Oic]NWGTa) demonstrated an EC_{50} of 4.97 x 10^{-8} M on the locust receptor and 1.15 x 10^{-7} M on the honeybee receptor in a separate trial (Fig. 1B). The Oic-AKH analog was thus only slightly less active as a honeybee receptor agonist than as a locust receptor agonist, suggesting that the unmodified Locmi-AKH-I would likely also interact well with the honeybee AKH receptor. A considerably higher concentration (EC_{50} = 7.06 x 10^{-6} M) of the cyclic analog was required to activate the locust receptor as compared to the native octapeptide (Schgr-AKH-II) and [Oic^5]Locmi-AKH-I analogs (Fig. 1), but it nonetheless displayed the same efficacy as the native peptide. In stark contrast, the cyclic analog exhibited only trace, if any, activity at 10^{-4} M on the honeybee receptor and no EC_{50} could be determined (Fig. 1). These results show that at pharmacological levels of application, the cyclic AKH analog selectively activates only the AKH receptor of the pest insect (desert locust) and not that of the beneficial insect (honeybee).

3.2 *NMR measurements*

The Spectral assignment and chemical shifts of both peptides are given in Table 1. For comparison, the NMR chemical shifts of linear-[LNFTPNWG-NH_2] in DMSO solution are reported as well. Linear-[LNFTPNWG-NH_2] was readily soluble in DPC micelle solution; this indicates that the peptide

334 interacts with the micelle. This interaction was confirmed by measuring the diffusion coefficient of
335 linear-[LNFTPNWG-NH_2] in DPC micelle solution. A value of 7×10^{-11} m^2s^{-1} was measured, which
336 is consistent with a micelle size of roughly 52 DPC molecules. Given the insensitivity of the diffusion
337 coefficient to molecular mass, this is in good agreement with our assumed size of 50 DPC molecules
338 per micelle but more importantly, justifies our use of the NOESY pulse sequence for such a small
339 peptide.

340 It is well known that proline prefers a trans configuration but sometimes exists in the cis form
341 (Alderson *et al.*, 2018). NMR is able to distinguish between these two configurations: trans-proline
342 shows strong NOEs between the two H_δ protons of proline and H_α and H^N of the preceding residue,
343 while cis-proline shows strong NOE between the two proline H_α protons and H_α of the preceding
344 residue. For both the linear and the cyclic peptide there was strong NOE between Trp^4 H_α and Pro^5
345 H_δ, confirming that both proline residues were in the trans configuration.

346 Structuring-induced chemical shift changes (observed shifts minus random coil reference values)
347 were analyzed using the CSDb algorithm (Eidenschink *et al.*, 2009). Different results were obtained
348 for the two peptides. For *cyclo*AKH (Figure 2a) the amide protons of residues 2-4 are shifted
349 downfield, while residues 6-8 are shifted up-field. The H_α, proton shifts are mainly shifted up-field.
350 Studies have shown that, with respect to their random coil values, both H_α and H^N are shifted up-
351 field by −0.30 ppm in helices, and downfield by ca. 0.6 ppm in β-sheets (Szilágyi, 1995). Thus, the
352 experimental chemical shifts obtained here (Fig. 2a) indicate that the dominant conformation of
353 *cyclo*AKH has a turn structure, which is expected in a cyclic peptide. These chemical shift changes
354 are similar to those found for Melme-CC, an octapeptide from the fruit beetle (*Pachnoda sinuata*)
355 and Declu-CC, a decapeptide from a blister beetle (*Decapotoma lunata*) (Jackson *et al.*, 2014) but
356 contrast with those found for Anoga-HrTH, an octapeptide from the malaria mosquito, *A. gambia*

(Mugumbate *et al.*, 2013). Tyndall *et al.* (2005) have reviewed the structure of over 100 ligands that bind to mammalian peptide–activated GPCRs, and found all of them to have turn structures.

Using the RCI tool (Berjanskii & Wishart, 2008) available on http://wishart.biology.ualberta.ca, the chemical shifts were also used to estimate the flexibility and the order parameter, S^2, of the peptide. A perfectly rigid structure has an order parameter of 1, while a completely flexible structure has an order parameter of 0. The results (Fig 2c) show that the cyclic peptide is very ordered, with a maximum order parameter of 0.85. This is similar to Melme-CC, Declu-CC and Anoga-HrTH, which are highly ordered, and have S^2 order parameters of 0.85, 0.7-0.9 and 0.7-0.8 respectively *(*Jackson *et al.*, 2014; Mugumbate *et al*., 2013).

The measured H^N temperature coefficients of *cyclo*AKH are given in Table 2. According to Baxter, H^N temperature coefficients of between -10 ppb/K and -6 ppb/K indicate the presence of transient or weak hydrogen bonds (Baxter & Williamson, 1997). Since the *cyclo*AKH is conformationally restricted and its temperature coefficients are between -7.1 and -9.6 ppb/K (Table 2), the presence of only weak hydrogen bonds is indicated.

For linear-[LNFTPNWG-NH_2], the random coil chemical shift deviations differed from those of *cyclo*AKH (Figure 2). Most of the residues have very small H^N shifts but large downfield shifts are seen for Phe^3 and Gly^8. Both up-field and downfield shifts are seen for H_α. Thus, the experimental chemical shifts indicate that the linear AKH peptide fragment has an extended (random coil) structure, with a possible turn structure at position 3 – 5. These results differ from our previous results on AKH peptides, where a turn structure was always found (see for example, Jackson *et al.*, 2019). While the chemical shift deviations from random coil values have been understood to indicate secondary structure, it is essential to point out that this interpretation is not unambiguous. Tremblay *et al.* (2010) have concluded that chemical shifts are more affected by the protein secondary structure than the solvent environment. The observation of a secondary structure are consistent with CD studies on

Locusta migratoria AKH neuropeptides, containing a proline residue, where a β-structure was proposed (Cusinato *et al*., 1998). Recent studies on Locmi-AKH-I also indicate a β-turn structure in DPC micelle solution (Jackson *et al.*, 2019).

The order parameters of linear-[LNFTPNWG-NH_2] are much lower than *cyclo*AKH (Fig. 2b) and are similar to those of Dappu-RPCH (Jackson *et al.*, 2018), which has an order parameter of only 0.25, thereby supporting the conclusion from the random coil chemical shift deviations of the current study that *cyclo*AKH is rigid while linear-[LNFTPNWG-NH_2] is flexible.

3.3 *Molecular Dynamic Analysis*

Since no meaningful NOE restraints were observed in the NMR spectra of *cyclo*AKH, all molecular dynamic simulations were done without restraints. The results are shown in Figure 3. Fig. 3a is an overlay of all the conformers collected during a 2 ns molecular dynamics simulation in water at 300K. As can be seen there is very little movement of the backbone but the side chains, especially the Trp and Phe side chains do move, although not as much as one would expect. Fig. 3b shows the backbone of the central conformer, which had a β type II turn around the proline. This turn structure is stabilized by transient polar contacts, two of which are shown in Figure 3b, between Asn^6(NH) and Thr^4(O); Asn^6(O) and Leu^1(NH); Thr^4(NH) and Leu^1(O); Asn^2(NH) and Gly^8(O). Note that all of the sidechains project out from the ring created by the backbone.

Following molecular dynamics in water, molecular dynamic simulations were also performed in DPC micelle solution. Cluster analysis of the trajectories gave a single large cluster. Figure 3c is an overlay of the two structures of *cyclo*AKH in water and DPC. As can be seen, the two structures are not perfectly aligned - the peptide backbone has changed slightly in DPC (Fig. 3c). The simulations were started with the peptide in the middle of the solvent box and the DPC micelle above and below it. Simulations were started with different orientations of the peptide relative to the DPC micelle so that different sidechains would interact with the DPC. In each case, the peptide diffused towards the

405 micelle and bound to its surface. The interaction between *cyclo*AKH and the micelle is shown in
406 Figure 3d.

407 Cluster analysis of the trajectory of linear-[LNFTPNWG-NH_2], in water, gave only one dominant
408 cluster (Figure 4). The peptide had an "extended" structure for the first three residues but a type IV β
409 -turn between residues 4–7. The β-turn is due to Pro^5. The overall structure is cyclic and is stabilized
410 by a moderately strong, transient H-bond between $Gly^8(NH_2)$ and $Asn^2(O_{\delta 1})$, $Gly^8(NH)$ and $Asn^6(O_{\delta 1})$,
411 $Gly^8(NH_2)$ and $Asn^6(CO)$, and $Gly^8(CO)$ and $Lys^1(NH_3)$. There is also a substantial amount of
412 hydrogen bonding between the peptide and the surrounding water molecules, which indicates the
413 structuring of water around the peptide. All the dihedral angles of the amino acids were in the allowed
414 region of dihedral space (not shown). It is perhaps surprising that such a short peptide should have
415 any structure, certainly the NMR results indicated that it was not structured (Fig. 2b). However, it
416 should be cautioned that the simulations were conducted with restraints derived from the NMR results
417 of the peptide in DPC micelle solution.

418 Cluster analysis of the trajectory of linear-[LNFTPNWG-NH_2], in DPC solution, also gave only one
419 large cluster. The structure in water and DPC solution is shown in Figure 4b. The two conformers are
420 very similar but the structure in DPC is more open and does not have the H-bonding between the
421 terminal residues. This is most probably because of the interaction with the micelle, which is shown
422 in Figure 4c.

423 One of the proposed hypotheses of GPCR binding is that the agonist first binds to the cell surface and
424 then moves across the surface until it encounters its receptor (Giragossian *et al*., 2002; Stone *et al.*,
425 2007a,b). Fascinatingly, this phenomenon is expressed in the molecular simulations of the current
426 study. One way of monitoring the interaction between the peptide and micelle is to calculate their area
427 of contact. This is shown in Figure 5, where the results for linear-[LNFTPNWG-NH_2] and *cyclo*AKH
428 are shown. For linear-[LNFTPNWG-NH_2], during the first 1 ns of the simulation, the peptide makes

429 occasional contact with the micelle surface, but after 40 ps is quite tightly bound to the surface. The
430 surface contact of the cyclic analog is quite different. As expected, the cyclic peptide/DPC interaction
431 depends on which residues are facing the micelle surface. This is shown in two simulations of the
432 cyclic peptide where the initial orientation of the peptide, relative to the DPC, was rotated through 180
433 degrees. In the one case, the peptide hardly interacts with the micelle (Fig. 5). With the other
434 orientation, the peptide becomes quite tightly bound and then moves away again (Fig. 5). At no time
435 does the cyclic peptide interact with the micelle to the same extent as the linear peptide. Since
436 *cyclo*AKH is constrained by its cyclic nature, it cannot change its conformation to maximize
437 interaction with the micelle surface. It is interesting to compare the simulations with Locmi-AKH-I,
438 the endogenous hormone upon which our two peptides were designed. Locmi-AKH-I has a very
439 similar surface contact area profile as linear-[LNFTPNWG-NH_2].

440 Figure 6 is an overlay of *cyclo*AKH, linear-[LNFTPNWG-NH_2] and Locmi-AKH-I. Here it is clear
441 that, even though the three peptides are very different they all have a very similar structure in micelle
442 solution. Locmi-AKH-I is a decapaptide but the first eight residues align well with the other two
443 peptides. This may account for *cyclo*AKH and Locmi-AKH-I (Jackson 2019) having similar activities
444 in the locust assay.

445 In order to investigate the structural similarity of *cyclo*AKH and linear-[LNFTPNWG-NH_2], they were
446 docked onto the *Schistocerca gregaria* receptor, Schgr-AKHR. The structural model of this receptor
447 was recently published, together with the Locmi-AKH-I binding site (Jackson, 2019). Glide docking
448 gave a glide score of -6.3 kJ/mol and -1.2 kJ/mol for *cyclo*AKH and linear-[LNFTPNWG-NH_2]
449 respectively. MMGBSA calculations on these two gave a binding free energy of -96 kJ/mol and -82
450 kJ/mol respectively. The docked structure of *cyclo*AKH is given in Figure 7, together with its ligand
451 interaction diagram. The ligand interaction diagram and binding site of linear-[LNFTPNWG-NH_2] is
452 given in Figure 8. These can be compared to the binding of Locmi-AKH-I (Figure 9) after MD
453 simulation in a phosphatidylcholine (POPC) membrane. The decapeptide lies in a cleft across the top

454 of the receptor (Figure 9) with the central portion of the peptide fitting into the binding pocket and the
455 two termini pointing outside the binding pocket. During the molecular dynamics, the terminal amide
456 was sometimes found to H-bond to a POPC molecule. The final binding energy for Locmi-AKH-I
457 was -98 kcal/mol, which is very similar to the other two peptides.

458 All three peptides are predicted to have the same binding site but differ in the details of their proposed
459 ligand/receptor interactions. These subtle differences can yield clues to the selectivity displayed by
460 *cyclo*AKH in its interaction with the locust receptor vs the honeybee receptor. All three peptides H-
461 bond to Gln^{287}. The linear peptides also interact with Trp^{87}. A complete list of ligand/receptor
462 interactions is given in Table 3. The *S. gregaria* AKH receptor is known to be more promiscuous,
463 accepting a number of different AKH-like agonists (see Gäde, 1990, and Marchal *et al.*, 2018).
464 Moreover, based on *in silico* predictions, all of the endogenous AKHs of the desert locust, i.e. Schgr-
465 AKH-II, Locmi-AKH-I and Aedae-AKH, were found to bind to the same binding site of Schgr-AKHR
466 (Jackson *et al.*, 2019).

467 3.4 *Apime*-AKHR

468 An important aspect of this research is the development of mimetic neuropeptide analogs that are
469 selective in their activity, negatively affecting the targeted pest species without harm to beneficial
470 insect species like the honeybee. *Cyclo*AKH demonstrates this selectivity in that it retains full efficacy
471 on a locust AKH receptor, while showing little or no activation of a honeybee AKH receptor. In order
472 to validate our computational results, *cyclo*AKH, linear-[LNFTPNWG-NH_2] and Locmi-AKH-I were
473 docked to a honeybee receptor. The recently published primary sequence of *Apime*-AKHR was
474 extracted from the Genbank database (accession number **AY898652**) and used to predict and model
475 the 3D structure of the honeybee receptor (Figure 1S). The highly conserved amino acid residues that
476 are common to Class A GPCRs (Chelikani *et al.*, 2007) were also present in *Apime*-AKHR (see Table
477 1S).

Since the primary structure indicated that not all the template could be used for the 3D modelling, three programs, PSIPRED 4.0, MEMSAT3/ MEMSAT-SVM (available at http://bioinf.cs.ucl.ac.uk/web_servers/) were used to predict the secondary structure. The result from PSIPRED indicated that only 317 of the 350 primary amino acid could be utilized for the construction of the 3D model (Figure 2S). MEMSAT-SVM confirmed this claim (Figure 3S). Having confirmed the composition and the primary amino acids that could form the 3D model of the molecule, SVM-GA topology analysis was used to predict the seven transmembrane (TMs) helical bundles and the loop regions (Figure 4S). Helices found were as follows: H1(39-61), H2 (77-102), H3 (110-140), H4 (156-172), H5 (203-225), H6 (261-282) and H7 (299-316). The pore-lining was found to be at residues 77-102, 110-140 and 399-316. The extracellular loops were ECL1(102-110), ECL2(172-203) and ECL3(282-299), while the cytoplasmic loops were ICL1(61-77), ICL2(140-156) and ICL3(225-261). A PSI_BLAST search gave the apelin receptor (5VBL) as the best template for the homology modeling of *Apime*-AKHR. The alignment of the *Apime*-AKHR amino acid sequence with the apelin receptor was relatively low in sequence identity (20 – 38%) but possess high sequence similarity (45 – 66%) (Table 2S). This is a common feature of the class A GPCR superfamily, where members with a low sequence identity but high sequence similarity have similar structures (Leach, 2001). The alignment of the *Apime*-AKHR amino acid sequence with the apelin receptor is shown in Figure 5S where the sequence identity and similarity are highlighted. There are no gaps in the alignment of the transmembrane regions. These regions had a relatively low sequence identity (20 – 38%) but had high sequence similarity (45 – 66%) (Table 2S). This is a common feature of the class A GPCRs superfamily, where members with a low sequence identity but high sequence similarity have similar structures (Leach, 2001).

Homology modeling based on the crystal structure of the apelin receptor gave the model shown in Figure 10. This model has 7 transmembrane helices with a tilted TM3. TM 4 is the shortest helix, while TM7 is the longest.

503 The quality of the constructed *Apime*-AKHR-model was assessed with the evaluation programs
504 ERRAT (Colovos and Yeates, 1993) and PROCHECK (Laskowski *et al*., 1996). A Ramachandran
505 plot, Figure 6S, showed that most of the amino acid residues are either in allowed or favored regions.
506 Also, the phi and psi, the backbone torsion angle, were acceptable. The ERRAT program gave a score
507 of 98.73. For a high-quality model the score must be >50 (Colovos and Yeates, 1993). Thus we
508 conclude that the *Apime*-AKHR-model is of high-quality and is acceptable for further study.
509 Figure 10 shows a comparison of the *Apime*-AKHR-model and the target template. As can be seen
510 there is very close agreement between the two. There are some differences, however. The *Apime*-
511 AKHR-model has 331 amino acid residues as against the template which has 389 amino acids. As a
512 result, TM6 and TM5 of the template are longer in length, with both helices extending by 4-5 residues
513 into the cytoplasm. This observation is consistent with studies conducted on the accessibility of
514 nitroxide labels fixed to ECL3 joining TM6 and TM5 of rhodopsin (Farahbakhsh, 1995). The
515 constructed model of *Apime*-AKH-R has the CWxP(Y/F) (CWTPY) motif in TM6; in the template
516 this sequence is CKMPY. In TM7 the constructed model has the (N/D)PxxY (NPIVY) motif, while in
517 the template it is NPFLY. These are the only significant differences noticed as regards the conserved
518 residues. These motifs are significant to receptor activations and will be discussed later. Also, the
519 constructed model has a disulphide bridge, commonly found in GPCRs, between Cys120 and Cys199.

520 Using the honeybee receptor, molecular docking of *cyclo*AKH, linear-[LNFTPNWG-NH_2] and *Locmi*-
521 AKH-I was performed. Docking with this receptor proved difficult as it has an unusually long ECL2,
522 which partially covers the entrance to the binding pocket. Also the binding pocket is quite restrictive.
523 The docking results showed that *cyclo*AKH (Figure 11a) was not able to enter the receptor binding site
524 and instead bound to the extracellular surface of the receptor. Its glide score was -4.6 with a binding
525 free energy of -0.4 kJ/mol. Blind docking of linear-[LNFTPNWG-NH_2] also proved difficult but after
526 minimising the docked structure a mmgbsa binding free energy of -128 kJ/mol was obtained. The
527 docked structure is shown in Figure 11b and the ligand interaction diagram in Figure 11c. For Locmi-

AKH-I, ΔG_{bind} was -148 kJ/mol (Figure 11c). Figure 11e shows details of the Locmi-AKH1 conformation when docked to *Apime*-AKHR. This is very similar to its conformation when bound to Schgr-AKHR (Figure 6). The ligand interaction diagram of Locmi-AKH-I bound to *Apime*-AKHR is shown in Figure 11f. Note the similarity in the ligand receptor interactions of linear-[LNFTPNWG-NH_2] and Locmi-AKH-I. Both hydrogen bond to Ser280, Ser126 and Tyr276. They both also have a π-π interaction with Phe302.

4. Concluding remarks

An NMR restrained, molecular dynamic study of a linear and head-to-tail cyclic, octapeptide AKH analog showed that the linear peptide was flexible in aqueous solution but had one preferred conformation when binding to a DPC micelle. This conformation was similar to the restricted conformation of the cyclic analog and the conformation of an endogenous AKH, Locmi-AKH-I. This may explain why *cyclo*AKH is able to activate the *in vitro*-expressed locust AKH receptor. Molecular docking calculations, using the published structure of the *S. gregaria* AKH receptor confirmed that all three peptides dock to the same binding site with very similar binding affinities. The cyclic constraints imposed on *cyclo*AKH may allow it to interact with the locust AKH receptor to a much greater extent than the honeybee receptor, where it demonstrates little or no activation. The locust AKH receptor has a greater tolerance for this conformational constraint, and this could suggest a greater tolerance for a shift in the direction of the type II β turn exhibited by *cyclo*AKH from the type IV β turn of the linear and native AKH peptides. Selectivity in mimetic analogs could potentially be enhanced by incorporating conformational constraints and residues that emphasize this shift. To obtain a more detailed explanation for the lack of tolerance of the honeybee receptor for *cyclo*AKH at the molecular level, the honeybee receptor, *Apime*-AKHR, was constructed and docked with *cyclo*AKH, linear-[LNFTPNWG-NH_2] and *Locmi*-AKH-I. *Locmi*-AKH-I, which activates this receptor, bound strongly

to the receptor, as did linear-[LNFTPNWG-NH_2]. However, *cyclo*AKH failed to enter the binding pocket and was only weakly bound to the honeybee receptor.

Acknowledgements

The authors acknowledge funding from the European Union's Horizon 2020 Research and Innovation programme under grant agreement No. 634361 (RJN, JVdB, HGM) (nEUROSTRESSPEP), the Research Foundation of Flanders (FWO) for providing a postdoctoral research fellowship to HV and a PhD fellowship to SS, and the Interuniversity Attraction Poles (IAP) programme (Belgian Science Policy Grant P7/40 to JVdB). Funding from the National Research Foundation of South Africa and UCT to HGM is also acknowledged (Grant No: 109204 [IFR170221223270]). The Centre for High-Performance Computing (CHPC), South Africa, provided computational resources for this research project. We are grateful to Prof. Marc Parmentier (Free University of Brussels, Belgium) and Dr. Michel Detheux (Euroscreen S.A., Belgium) for providing CHO-WTA11 cells.

References

Abraham, M.J., Murtola, T., Schulz, R., Páll, S., Smith, J.C., Hess, B., Lindahl, E., 2015. GROMACS: High-performance molecular simulations through multi-level parallelism from laptops to supercomputers. *SoftwareX 1–2*, 19–25. https://doi.org/10.1016/J.SOFTX.2015.06.001

Alderson T.R., Lee J.H., Charlier C., Ying J., Bax A., 2018. Propensity for cis-Proline Formation in Unfolded Proteins. *Chembiochem*, 19(1), 37-42. doi: 10.1002/cbic.201700548

Altschul, S.F., Gish, W., Miller, W., Myers, E.W., Lipman, D.J., 1990. Basic local alignment search tool., *J. Mol. Biol. 215*, 403–10.

Audsley, N., Down, R.E. 2015. G-protein coupled receptors as targets for next generation pesticides. *Insect Biochem. Mol. Biol. 67*, 27-37.

Baxter N.J., Williamson M.P., 1997. Temperature dependence of 1H chemical shifts in proteins. *J Biomol NMR. 9*(4),359-69.

Beenakkers, A.M.T., Bloemen, R.E.B., De Vlieger, T.A., Van Der Horst, D.J., Van Marrewijk, W.J.A., 1985. Insect adipokinetic hormones. *Peptides 6*(SUPPL. 3), 437–444. https://doi.org/10.1016/0196-9781(85)90411-5

Berjanskii, M.V, & Wishart, D.S., 2008. Application of the random coil index to studying protein flexibility. *Journal of Biomolecular NMR*. *40*(1), 31-48. https://doi.org/10.1007/s10858-007-9208-0

582 Berman, H.M., 2008. IUCr. The Protein Data Bank: a historical perspective. *Acta Crystallogr. Sect. A.*
583 *64*, 88-95.

584 Berman, H.M., Kleywegt, G.J., Nakamura, H., J. L. Markley, J.L., The Protein Data Bank archive as
585 an open data resource, *J. Comput. Aided. Mol. Des.*, , DOI:10.1007/s10822-014-9770-y.

586 BLAST, BLAST Basic Local Alignment Search Tool.

587 Braunschweiler, L., & Ernst, R.R., 1983. Coherence transfer by isotropic mixing: Application to proton
588 correlation spectroscopy. *Journal of Magnetic Resonance 53*(3), 521–528.
589 https://doi.org/10.1016/0022-2364(83)90226-3

590 Chelikani P., Hornak V., Eilers M., Reeves P.J., Smith S.O., Raj Bhandary U.L., and Khorana H.G.,
591 2007. Role of group-conserved residues in the helical core of β_2-adrenergic receptor. *Proc. Natl.*
592 *Acad. Sci. U. S. A.* 104(17), 7027–7032.

593 Colovos, C., Yeates, T. O., 1993. Verification of Protein Structures: Patterns of Nonbonded Atomic
594 Interactions. Protein Sci., 2 (9), 1511–1519. https://doi.org/10.1002/pro.5560020916.
595
596 Cusinato, O., Drake, A.F., Gäde, G., Goldsworthy, G.J., 1998. The molecular conformations of
597 representative arthropod adipokinetic peptides determined by circular dichroism spectroscopy.
598 *Insect Biochemistry and Molecular Biology*. *28*(1), 43-50. https://doi.org/10.1016/S0965-
599 1748(97)00094-5
600
601 Delano, W.L., 2002. The PyMOL Molecular Graphics System, *http://www.pymol.org*,
602 https://ci.nii.ac.jp/naid/10020095229/ (2002, accessed 7 August 2018).
603
604 Eidenschink, L., Kier, B.L. , Huggins, K.N.L. , Andersen, N.H., 2009. Very short peptides with stable
605 folds: Building on the interrelationship of Trp/Trp, Trp/cation, and Trp/backbone-amide
606 interaction geometries. *Proteins Struct Funct Bioinforma. 75*, 308–322.
607
608 Farahbakhsh Z.T., Ridge K.D., Khorana H.G., Hubbell W.L., 1995. Mapping Light-Dependent Structural
609 Changes in the Cytoplasmic Loop Connecting Helixes C and D in Rhodopsin: A Site-Directed Spin
610 Labeling Study. *Biochemistry*. *34*, 8812-8819. doi:10.1021/bi00027a033

611
612 Gäde, G., 1990. Structure–function studies on hypertrehalosaemic and adipokinetic hormones: activity
613 of naturally occurring analogues and some N- and C-terminal modified analogues. Physiological
614 Entomology. 15(3):229-316.
615
616 Gäde, G., 2005. Adipokinetic hormones and the hormonal control of metabolic activity in Hemiptera.
617 *Pestycydy* (4), 49–54.

618 Gäde, G., 2004. Regulation of intermediary metabolism and water balance of insects by neuropeptides.
619 *Annu. Rev. Entomol*. *49*, 93–113. https://doi.org/10.1146/annurev.ento.49.061802.123354

620 Gäde, G., 2009. Peptides of the adipokinetic hormone/red pigment-concentrating hormone family: A
621 new take on biodiversity. In *Annals of the New York Academy of Sciences* (Vol. 1163, pp. 125–
622 136). https://doi.org/10.1111/j.1749-6632.2008.03625.x

623 Gäde, G., Goldsworthy, G.J. 2003. Insect peptide hormones: a selective review of their physiology and
624 potential application for pest control. *Pest Management Sci. 59*, 1063-1075.

625 Gäde, G., & Marco, H.G., 2006. Structure, Function and Mode of Action of Select Arthropod

626 Neuropeptides. *Studies in Natural Products Chemistry 33*, 69–139.
627 https://doi.org/10.1016/S1572-5995(06)80026-8

628 Gäde, G., & Marco, H.G., 2013. Chapter 28 – AKH/RPCH Peptides. In *Handbook of Biologically*
629 *Active Peptides* (pp. 185–190). https://doi.org/10.1016/B978-0-12-385095-9.00028-2

630 Gäde, G., Šimek, P., Marco, H.G., 2017. The African froghopper *Ptyelus flavescens* (suborder:
631 Cicadomorpha) contains two novel and one known peptides of the adipokinetic hormone (AKH)
632 family: structure, function and comparison with aphid AKH (suborder: Sternorrhyncha. *Amino*
633 *Acids 49(10),* 1679-1690. https:// doi:10.1007/s00726-017-2461-y

634 Giragossian, C., Pellegrini, M., Mierke, D.F., 2002. NMR studies of CCK-8/CCK1 complex support
635 membrane-associated pathway for ligand-receptor interaction. *Canadian Journal of Physiology*
636 *and Pharmacology*. https://doi.org/10.1139/Y02-031

637 Goldsworthy, G., Opoku-Ware, K., Mullen, L., 2002. Adipokinetic hormone enhances laminarin and
638 bacterial lipopolysaccharide-induced activation of the prophenoloxidase cascade in the African
639 migratory locust, *Locusta migratoria*. *Journal of Insect Physiology 48*(6), 601–608.
640 https://doi.org/10.1016/S0022-1910(02)00085-9

641 Guex, N., Peitsch, M.C., 1997. SWISS-MODEL and the Swiss-PdbViewer: An environment for
642 comparative protein modeling, *Electrophoresis*. *18*, 2714-2723.
643 DOI:10.1002/elps.1150181505.

644 Guex, N., Peitsch, M.C., Schwede, T., 2009. Automated comparative protein structure modeling with
645 SWISS-MODEL and Swiss-PdbViewer: A historical perspective, *Electrophoresis*. *30*, S162–
646 S173.

647 Jackson, G.E., Mabula, A.N., Stone, S.R., Gäde, G., Kövér, K.E., Szilágyi, L., & van der Spoel, D.,
648 2009. Solution conformations of an insect neuropeptide: Crustacean cardioactive peptide
649 (CCAP). *Peptides 30*(3), 557–564. https://doi.org/10.1016/J.PEPTIDES.2008.11.014

650 Jackson, G.E., Pavadai, E., Gerd G., Andersen, N.H., 2019. The adipokinetic hormones and their
651 cognate receptor from the desert locust, *Schistocerca gregaria*: solution structure of endogenous
652 peptides and models of their binding to the receptor. *PeerJ*, 7, e7514. DOI 10.7717/peerj.7514
653
654 Jackson, G.E., Pavadai, E., Gäde, G., Timol, Z., Andersen, N.H., 2014. Structural studies of
655 adipokinetic hormones in water and DPC micelle solution using NMR distance restrained
656 molecular dynamics. *Peptides*, *53*, 270–277.
657
658 Jackson, G.E., Pavadai, E., Gerd G., Timol Z., Andersen, N.H., 2018. Interaction of the red pigment-
659 concentrating hormone of the crustacean *Daphnia pulex*, with its cognate receptor, Dappu-
660 RPCHR: A nuclear magnetic resonance and modeling study, *International Journal of Biological*
661 *Macromolecules*. *106*, 969 – 978, https://doi.org/10.1016/j.ijbiomac.2017.08.103.

662 Jeener, J., Meier, B.H, Bachmann, P., Ernst, R.R., 1979. Investigation of exchange processes by two-
663 dimensional NMR spectroscopy. *J.Chem. Phys*. *71*, 4556-4559.
664 https://doi.org/10.1063/1.438208

665 Jones, D.T., 2007. Improving the accuracy of transmembrane protein topology prediction using
666 evolutionary information, *Bioinformatics*. *23*, 538–544.

667 Kaczmarek, K., Williams, H.J., Coast, G. M., Scott, A.I., Zabrocki, J., Nachman, R.J., 2007.
668 Comparison of insect kinin analogs with cis-peptide bond motif 4-aminopyroglutamate identifies

669 optimal stereochemistry for diuretic activity. *Biopolymers (Peptide Sci.) 88*, 1-7. https://doi.org/
670 10.1002/bip.20613
671
672 Laskowski R.A., Rullmann J.A.C., MacArthur M.W., Kaptein J.M.R., 1996. AQUA and
673 PROCHECK-NMR: Programs for checking the quality of protein structures solved by NMR.
674 J. Biomol. NMR, 8, 477. doi:10.1007/BF00228148

675 Leach, A. R., 2001. Molecular Modelling: Principles and Applications (2nd Edition), Prentice Hall.
676 https://doi.org/10.1016/S0097-8485(96)00029-0.

677 Lorenz, M.W., & Gade, G., 2009. Hormonal regulation of energy metabolism in insects as a driving
678 force for performance. *Integrative and Comparative Biology 49*(4), 380–392.
679 https://doi.org/10.1093/icb/icp019

680 Ma, Y., Yue, Y., Ma, Y., Zhang, Q., Zhou, Q., Song, Y., Shen, Y., Li, X., Ma, X., Li, C., Hanson,
681 M.A., Han, G.W., Sickmier, E.A., Swaminath, G., Zhao, S., Stevens, R.C., Hu, L.A., Zhong,
682 W., Zhang, M., Xu, F., 2017. Structural Basis for Apelin Control of the Human Apelin
683 Receptor, *Structure*. *25*, 858-866. DOI:10.1016/j.str.2017.04.008.

684 Marchal, E., Schellens, S., Monjon, E., Bruyninckx, E., Marco, H.G., Gäde, G., Vanden Broeck, J.,
685 Verlinden, H., 2018. Analysis of Peptide Ligand Specificity of Different Insect Adipokinetic
686 Hormone Receptors. *International Journal of Molecular Sciences 19*(2).
687 https://doi.org/10.3390/ijms19020542

688 Marco, H.G., & Gäde, G., 2015. Structure-activity relationship of adipokinetic hormone analogues in
689 the striped hawk moth, *Hippotion eson*. *Peptides 68*, 205–210.
690 https://doi.org/10.1016/j.peptides.2015.01.007

691 Marco, H.G., Šimek, P., Clark, K.D. and Gäde, G. 2013. Novel adipokinetic hormones in the kissing
692 bugs *Rhodnius prolixus*, *Triatoma infestans*, *Dipetalogaster maxima* and *Panstrongylus megistus*.
693 Peptides 41, 21–30. http://dx.doi.org/10.1016/j.peptides.2012.09.032

694 McGuffin, L.J., Bryson, K., Jones, D.T., 2000. The PSIPRED protein structure prediction server.,
695 *Bioinformatics. 16*, 404–5.

696 Moyna, G., Williams, H.J., Nachman, R.J., 1999a. Conformation in solution and dynamics of a
697 structurally constrained linear insect kinin pentapeptide analogue. *Biopolymers 49*, 403-413.
698
699 Moyna, G., Williams, H.J., Nachman, R.J., Scott, A.I., 1999b. Detection of nascent polyproline II
700 helices in solution by NMR in synthetic insect kinin neuropeptide mimics containing the X-Pro-
701 Pro-X motif. *J. Pept. Res. 53*, 294-301.
702
703 Mugumbate, G., Jackson, G.E., van der Spoel, D., Kövér, K.E., Szilágyi, L., 2013. *Anopheles gambiae*,
704 Anoga-HrTH hormone, free and bound structure – A nuclear magnetic resonance experiment,
705 *Peptides*. *41*,94–100.
706
707 Nachman, R.J., 2009a. Agonists/antagonists of the insect kinin and pyrokinin/PBAN neuropeptide
708 classes as tools for rational pest control, pp. 21-48. In Ishaaya, I. and Horowitz, A.R. (eds.).
709 Biorational Control of Arthropod Pests: Application and Resistance Management, Springer, The
710 Netherlands. 408 pp.
711
712 Nachman, R.J., 2014a. Mimetic analogs of pyrokinin neuropeptides for pest management'. In: Gross
713 A.D., Coats J.R., Duke S.O., Seiber J. Biopesticides: State of the Art and Future Opportunities,
714 Chapter 7, pp. 71-81, American Chemical Society, Washington D.C.

Nachman R.J., 2014b. Applied peptidomics: A new strategy for the development of antagonists and/or selective agonists of the insect pyrokinin (FXPRLamide) superfamily using a novel conformational-mimetic motif. *EuPA Open Proteomics 3*, 138-142. https://doi.org/ 0.1016/j.euprot.2014.02.008

Nachman, R.J., Ben-Aziz, O., Davidovitch, M., Kaczmarek, K., Zabrocki, J., Williams, H., Strey, A.A., Altstein, M., 2010. A novel dihydromidazoline, trans-Pro mimetic analog is a selective PK/PBAN agonist. *Front. Biosci. E2*, 195-203. https://doi.org/10.2741/E82

Nachman, R.J., Kim, Y., Wang, X.J., Etzkorn, F.A., Kaczmarek, K., Zabrocki, J., Adams, M.E., 2009b. Potent activity of a PK/PBAN analog with an (E)-alkene, trans-Pro mimic identifies the Pro orientation and core conformation during interaction with HevPBANR-C receptor. *Bioorg. Med. Chem. 17*, 4216-4220. https://doi.com/ 10.1016/j.bmc.2009.03.036

Nachman, R.J., Moyna, G., Williams, H.J., Tobe, S.S., Scott, A.I., 1998. Synthesis, biological activity, and conformational studies of insect allatostatin neuropeptide analogs incorporating turn promoting moieties. *Bioorg. Med. Chem. 6*, 1379-1388. https://doi.org/10.1016/S0968-0896(98)00129-1

Nachman, R.J. and Pietrantonio, P. V., 2010. Interaction of mimetic analogs of insect kinin neuropeptides with arthropod receptors, pp. 86-98. In Geary, T.G. and Maule, A.G. (eds.). Neuropeptide Systems as Targets for Parasite and Pest Control, Landes Bioscience, Austin, TX. 230 pp.

Nachman, R.J., Roberts, V.A., Dyson, H.J., Holman, G.M., Tainer, J.A., 1991. Active conformation of an insect neuropeptide family. *Proc. Natl. Acad. Sci. USA. 88*, 4518-4522. https://doi.org/ 10.1073/pnas.88.10.4518

Nachman, R.J., Wang, X.J., Etzkorn, F.A., Ben-Aziz, O., Davidovitch, M., Kaczmarek, K., Zabrocki, J., Strey, A.A., Pryor, N.W., Altstein, M., 2009c. Evaluation of a PK/PBAN analog with an (E)-alkene, *trans*-Pro isostere identifies the Pro orientation for activity in four diverse pyrokinin bioassays. *Peptides 30*, 1254-1259. https://doi.org/10.1016/j.peptides.2009.04.017

Nachman, R.J., Wang, X.J., Etzkorn, F.A., Kaczmarek, K., Zabrocki, J., Lopez, J. D., Coast, G. M., 2013. Evaluation of insect CAP2b analogs with either an (*E*)-alkene, *trans*- or a (*Z*)-alkene, *cis*-Pro isostere identifies the Pro orientation for antidiuretic activity in the stink bug. *Peptides 41*, 101-106. https://doi.org/ 10.1016/j.peptides.2012.09.026

Nachman, R.J., Zabrocki, J., Olczak, J., Williams, H.J., Moyna, G., Scott, A.I.., Coast, G.M., 2002. *cis*-Peptide bond mimetic tetrazole analogs of the insect kinins identify the active conformation. *Peptides 23*, 709-716.

Offermanns, S., Simon, M.I. (1995). G alpha 15 and G alpha 16 couple a wide variety of receptors to phospholipase C. *J. Biol. Chem. 270*(25), 15175-15180. https://doi.org/10.1074/jbc.270.25.15175

Park, Y., Kim, Y.J., Adams, M.E. 2002. Identification of G-protein-coupled receptors for Drosophila PRX-amide peptides, CCAP, corazonin, and AKH supports a theory of ligand receptor coevolution. *Proc. Natl. Acad. Sci. USA 99*, 11423-11428.

764 Roberts, V.A., Nachman, R.J., Coast, G.M., Chung, J.S., Holman, G.M., Hariharan, M., Tainer, J.A.,
765 1997. Concensus chemistry and conformation of the active core of the myotropic/diuretic insect
766 kinin neuropeptide family from experimental data and molecular dynamics. *Chem. Biol. 4*, 105-
767 117.
768
769 Sklenar, V., & Bax, A., 1987. A new water suppression technique for generating pure-phase spectra
770 with equal excitation over a wide bandwidth. *Journal of Magnetic Resonance (1969)*, *75*(2), 378–
771 383. https://doi.org/10.1016/0022-2364(87)90046-1

772 Sklenar, V., Piotto, M., Leppik, R., Saudek, V., 1993. Gradient-Tailored Water Suppression for 1H-
773 15N HSQC Experiments Optimized to Retain Full Sensitivity. *Journal of Magnetic Resonance,*
774 *Series A 102*(2), 241–245. https://doi.org/https://doi.org/10.1006/jmra.1993.1098

775 Stables, J., Green, A., Marshall, F., Fraser, N., Knight, E., Sautel, M., Milligan, G., Lee, M., Rees, S.,
776 1997. A bioluminescent assay for agonist activity at potentially any G-protein-coupled receptor.
777 *Anal. Biochem. 252*(1), 115-126. https://doi.org/10.1006/abio.1997.2308

778 Standfuss J, Edwards PC, D'Antona A, Fransen M, Xie G, Oprian DD, Schertler GF. 2011. The
779 structural basis of agonist-induced activation in constitutively active rhodopsin. *Nature. 471*,
780 656–660. DOI:10.1038/nature09795.

781 Staubli, F., Jorgensen, T.J.D., Cazzamali, G., Williamson, M., Lenz, C., Sendergaard, L., et al. 2002.
782 Molecular identification of the insect adipokinetic hormone receptors. *Proc. Natl. Acad. Sci.*
783 *USA. 99*, 3446-3451.

784 Stone, S.R., Giragossian, C., Mierke, D.F., Jackson, G.E., 2007a. Further evidence for a C-terminal
785 structural motif in CCK2receptor active peptide hormones. *Peptides*. *28*(11), 2211-2222.
786 https://doi.org/10.1016/j.peptides.2007.09.008

787 Stone, S.R., Mierke, D.F., Jackson, G. E., 2007b. Evidence for a C-terminal structural motif in gastrin
788 and its bioactive fragments in membrane mimetic media. *Peptides 28*(8), 1561–1571.
789 https://doi.org/10.1016/J.PEPTIDES.2007.07.009

790 Stone, J.V., Mordue, W., Batley, K.E., Morris, H.R., 1976. Structure of locust adipokinetic hormone,
791 a neurohormone that regulates lipid utilisation during flight. *Nature 263*(5574), 207–211.
792 https://doi.org/10.1038/263207a0

793 Szilágyi, L, 1995. Chemical shifts in proteins come of age. Prog Nucl Magn Reson Spectrosc. *27 (4)*,
794 325-442.

795 Taneja-Bageshwar, S., Strey, A.A., Isaac, R.E., Coast, G.M., Zubrzak, P., Pietrantonio, P.V.,
796 Nachman, R.J. 2009. Biostable agonists that match or exceed activity of native insect kinins on
797 recombinant arthropod GPCRs. *Gen. Comp. Endocrinol. 162*, 122-128.
798 doi:10.1016/j.ygcen.2008.10.013

799 Taneja-Bageshwar, S., Strey, A.A., Kaczmarek, K., Zabrocki, J., Pietrantonio, P., Nachman, R.J.,
800 2008. Comparison of insect kinin analogs with cis-peptide bond, type VI-turn motifs identifies
801 optimal tereochemistry for interaction with a recombinant arthropod kinin receptor from the
802 southern cattle tick, *Boophilus microplus*. *Peptides 29*, 295-301.
803 https://doi.org/10.1016/j.peptides.2007.09.024

804 Thomas, P.D., Basus, V.J., James, T.L., 1991. Protein solution structure determination using distances
805 from two-dimensional nuclear Overhauser effect experiments: effect of approximations on the
806 accuracy of derived structures. *Proceedings of the National Academy of Sciences of the United*

States of America 88(4), 1237–1241. Retrieved from http://www.ncbi.nlm.nih.gov/pubmed/1996325

Tieleman, D.P., van der Spoel, D., & Berendsen, H.J.C., 2000. Molecular dynamics simulations of dodecylphosphocholine micelles at three different aggregate sizes: Micellar structure and chain relaxation. *The Journal of Physical Chemistry B*., 104(27), 6380-6388. https://doi.org/10.1021/jp001268f

Tremblay, M.L., Banks, A.W., Rainey, J.K., 2010. The predictive accuracy of secondary chemical shifts is more affected by protein secondary structure than the solvent environment. *Journal of Biomolecular NMR*. *46,* 257-262. https://doi.org/10.1007/s10858-010-9400-5

Tyndall, J.D.A., Pfeiffer, B., Abbenante, G., Fairlie, D.P., 2005. Over one hundred peptide-activated G protein-coupled receptors recognize ligands with turn structure. *Chem. Rev. 105*, 793–826.

Van Der Spoel, D., Lindahl, E., Hess, B., Groenhof, G., Mark, A.E., Berendsen, H.J.C., 2005. GROMACS: Fast, flexible, and free. *Journal of Computational Chemistry*. *26*(16), 1701-1718. https://doi.org/10.1002/jcc.20291

Verlinden, H., Vleugels, R., Zels, S., Dillen, S., Lenaerts, C., Crabbé, K., Spit, J., Vanden Broeck, J. (2014). Receptors for neuronal or endocrine signalling molecules as potential targets for the control of insect pests. Advances in Insect Physiology 46, 167-303.

Vohra S., Taddese B., Conner A.C., Poyner D.R., Hay D.L., Barwell J., Reeves P.J., Upton G.J.G., Reynolds C.A., 2013. Similarity between class A and class B G-protein-coupled receptors exemplified through calcitonin gene-related peptide receptor modelling and mutagenesis studies. *J R Soc Interface. 10*, 20120846. http://dx.doi.org/10.1098/rsif.2012.0846.

Waterhouse, A., Bertoni, M., Bienert, S., Studer, G., Tauriello, G., Gumienny, R., Heer, F.T., De Beer, T.A.P., Rempfer, C., Bordoli, L., Lepore, R., Schwede, T., 2018. SWISS-MODEL: Homology modelling of protein structures and complexes, *Nucleic Acids Res. 46*, W296–W303. https://doi.org/10.1093/nar/gky427.

Weber, P.L., Morrison, R., Hare, D., 1988. Determining stereo-specific 1H nuclear magnetic resonance assignments from distance geometry calculations. *Journal of Molecular Biology 204*(2), 483–487. https://doi.org/10.1016/0022-2836(88)90589-X

Wüthrich, K., 1986. NMR of Proteins and Nucleic Acids. *Society* (Vol. 32), New York: Wiley.. https://doi.org/10.1039/b618334b

Yang, H., Huang, J., Liu, Y., Li, J., S. Luo, S., J. Wu, J., 2018. Prediction of the post-translational modifications of adipokinetic hormone receptors from solitary to eusocial bees, *Sociobiology*. *65*, 271–279.

Zhang, Q., Nachman, R.J., Zubrzak, P., Denlinger, D.L., 2009. Conformational aspects and hyperpotent agonists of diapause hormone for termination of pupal diapause in the corn earworm. *Peptides 30*, 596-602. https://doi.org/10.1016/j.peptides.2008.07.006

Zhang, Q., Nachman, R.J., Kaczmarek, K., Zabrocki, J., Denlinger, D.L., 2011. Disruption of insect diapause using agonists and an antagonist of diapause hormone. *Proc. Natl. Acad. Sci. USA 108*, 16922-16926. https://doi.org/ 10.1073/pnas.1113863108

Figure Legends

Figure 1. Dose-response curves of AKH peptides and analogs measured in a Ca^{2+} dependent, aequorin-based, bioluminescence reporter assay for the honeybee (*Apime*AKHR; left panels) or the desert locust (*Schgr*AKHR; right panels) AKH receptor. These receptors were expressed in CHO cells together with the bioluminescent Ca^{2+} reporter protein aequorin and the promiscuous Ga_{16} subunit. Data are shown as means ± SD. The % of bioluminescence, indicated on the y-axis, is used to approximate the activity of the respective receptors relative to the highest signal observed during the assay, as obtained with 1µM *Schgr*-AKH-II. The zero % (blank level) refers to the bioluminescence detected when cells were combined with medium containing 0.1% BSA without agonist. The logarithm of the molar ligand concentration is shown on the x-axis. Every experiment was performed at least twice. Panel A the naturally occurring agonists *Schgr*-AKH-I (pQLNFTPNWGTa) and *Schgr*-AKH-II (pQLNFSTGWa); panel B compares *Schgr*-AKH-II (pQLNFSTGWa = *Schgr*-AKH-II = *Apime*-AKH) with two synthetic AKH-I analogs, pQLNFT[Oic]NWGTa and *cyclo*(LNFTPNWG).

Figure 2. Random coil chemical shift deviation (a) *cyclo*AKH, (b) linear-[LNFTPNWG], (c) S^2 order parameter.

Figure 3. a) Overlay of main *cyclo*AKH cluster from trajectory in water (b) Lowest energy conformation of *cyclo*AKH in water; c) overlay of lowest energy conformation of *cyclo*AKH in water (green ribbon) and DPC (red ribbon) solution; (d) *cyclo*AKH interacting with a DPC micelle.

Figure 4. a) Two views of linear-[LNFTPNWG-NH2] in water showing H-bonds; (b) comparison of *cyclo*AKH in water and linear-[LNFTPNWG-NH2] in dpc; (c) linear-[LNFTPNWG-NH2] bound to dpc micelle.

Figure 5. Solvent accessible surface area for three different peptides in DPC micelle solution as a function of time. Note that for *cyclo*AKH the molecular dynamics was started with two different orientations of the peptide relative to the micelle.

Figure 6. Overlay of *cyclo*AKH, linear-[LNFTPNWG-NH_2] and Locmi-AKH-I. *Cyclo*AKH and linear-[LNFTPNWG-NH_2] are colored according to residue position, while *Locmi*-AKH-I is colored normally.

Figure 7. *Cyclo*AKH docked to the *Schistocerca gregaria* receptor, *Schgr*-AKHR. Expansion of docked structure and ligand interaction diagram.

Figure 8. linear-[LNFTPNWG-NH_2] docked to the *Schistocerca gregaria* receptor, *Schgr*-AKHR. Expansion of docked structure and ligand interaction diagram.

Figure 9. *Locmi*-AKH-I docked to *Schistocerca gregaria* receptor, *Schgr*-AKHR, showing the binding site surface of the receptor. (b) Ligand interaction diagram for *Locmi*-AKH-I and *Schgr*-AKHR.

Figure 10. An overlay of *Apime*-AKHR-model (in green) with the apelin receptor crystal structure (in yellow).

Figure 11. *Apime*-AKHR (a) in popc membrane with *cyclo*AKH docked at the surface. (b) Expansion showing docked linear-[LNFTPNWG-NH_2]. (c) Ligand interaction diagram of linear-[LNFTPNWG-NH_2]. (d) *Locmi*-AKH1 docked. (e) docked conformation of *Locmi*-AKH-1. (f) Ligand interaction diagram of *Locmi*-AKH1. The ligand is displayed as a 2D structure. Interactions between the residues and the ligand are drawn as lines, colored by interaction type, purple for H-bonding and green for π-π stacking. The binding pocket is indicated by a line drawn around the ligand, colored by the color of the nearest residue. Solvent exposure is indicated on the ligand atoms, and by the break in the line drawn around the pocket.

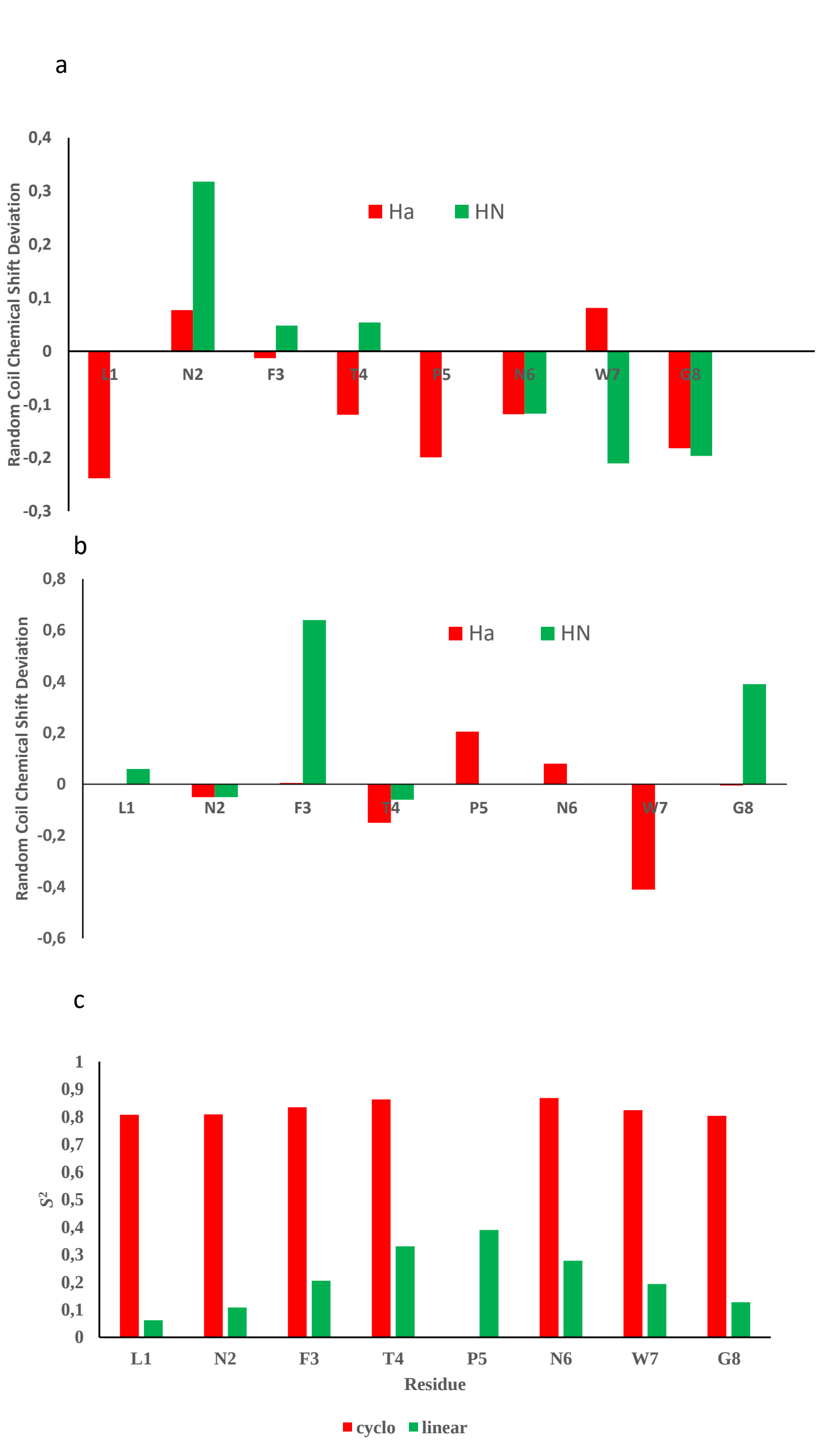
a
0,4
0,3
0,2
0,1
0
-0,1
-0,2
-0,3
Random Coil Chemical Shift Deviation
Ha
HN
L1
N2
F3
T4
P5
N6
W7
G8
b
0,8
0,6
0,4
0,2
0
-0,2
-0,4
-0,6
Random Coil Chemical Shift Deviation
Ha
HN
L1
N2
F3
T4
P5
N6
W7
G8
c
1
0,9
0,8
0,7
0,6
0,5
0,4
0,3
0,2
0,1
0
S2
L1
N2
F3
T4
P5
N6
W7
G8
Residue
cyclo
linear

a

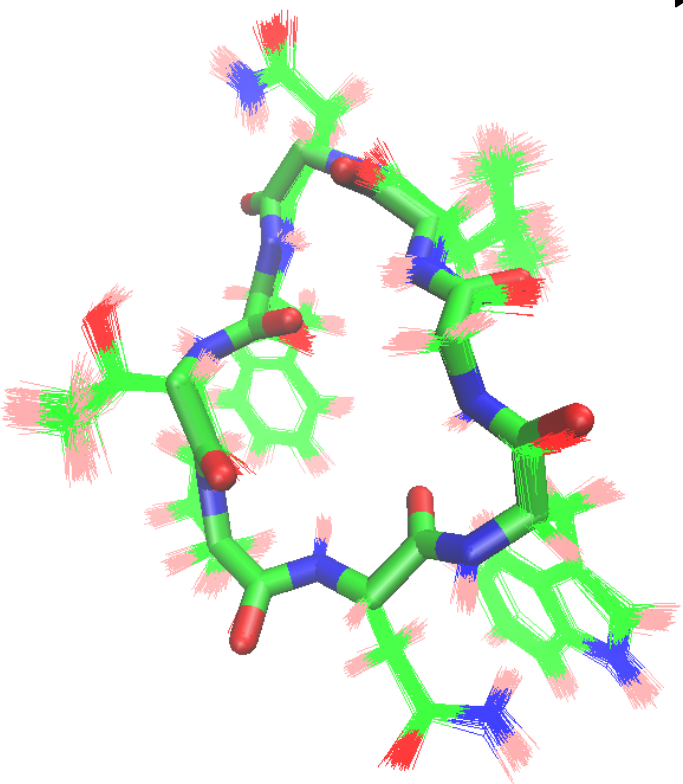

b

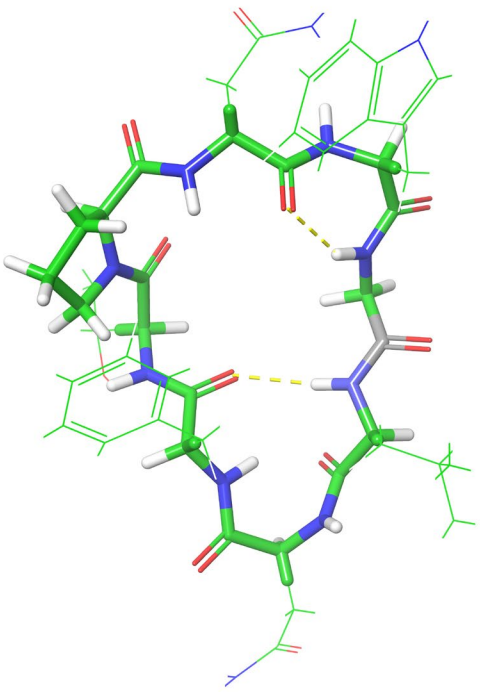

c

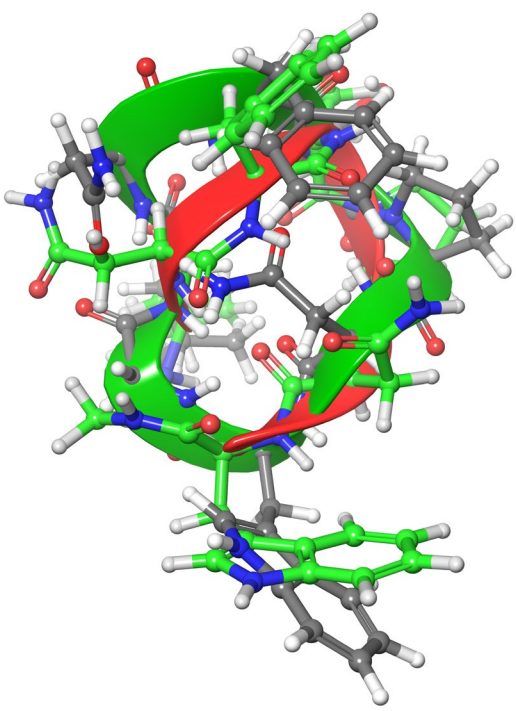

d

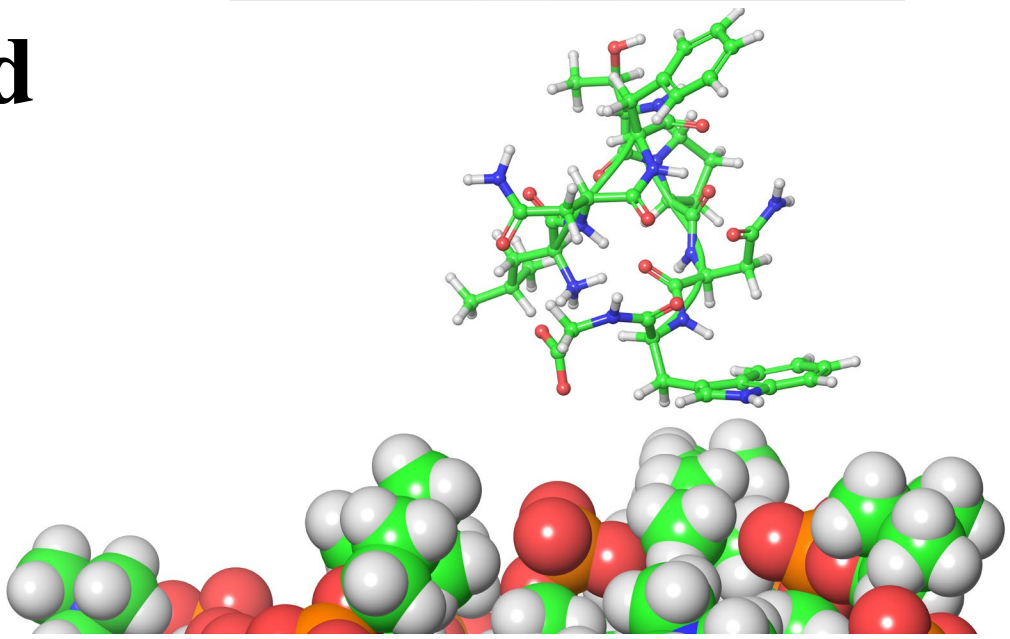

a

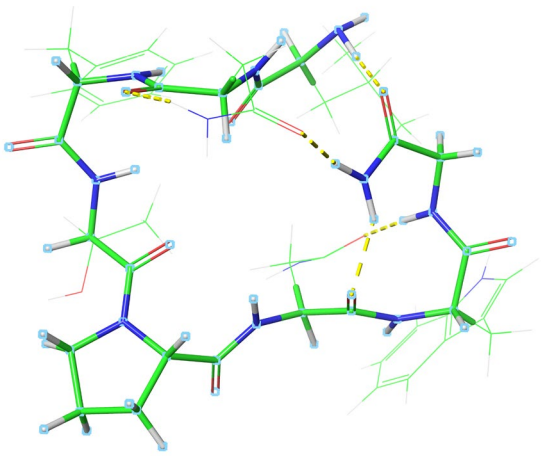

Top view

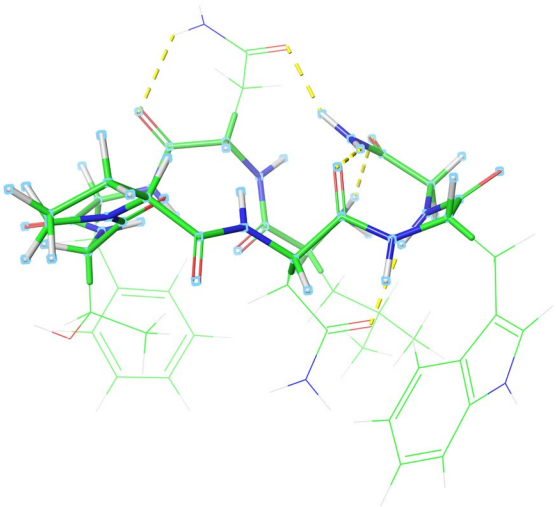

Side view

b

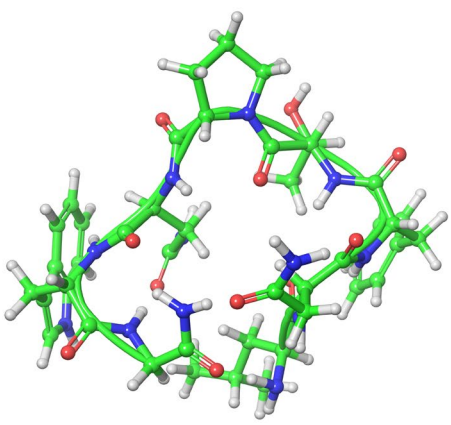

water

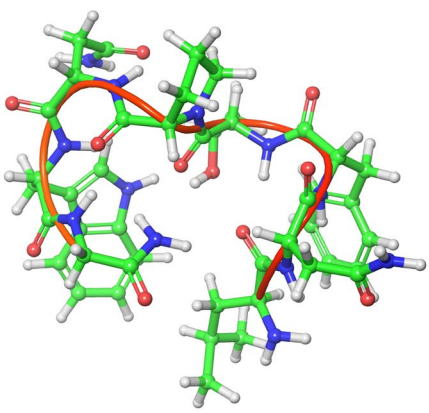

DPC

c

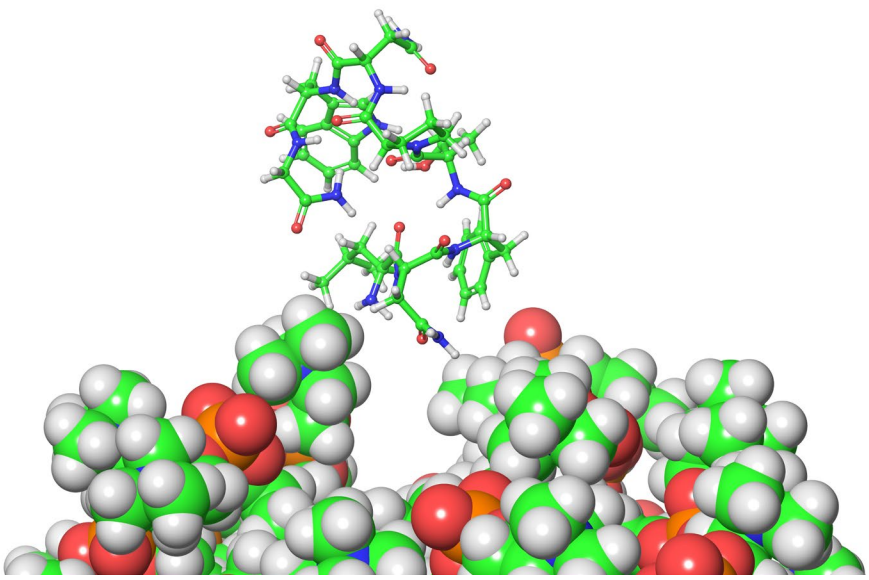

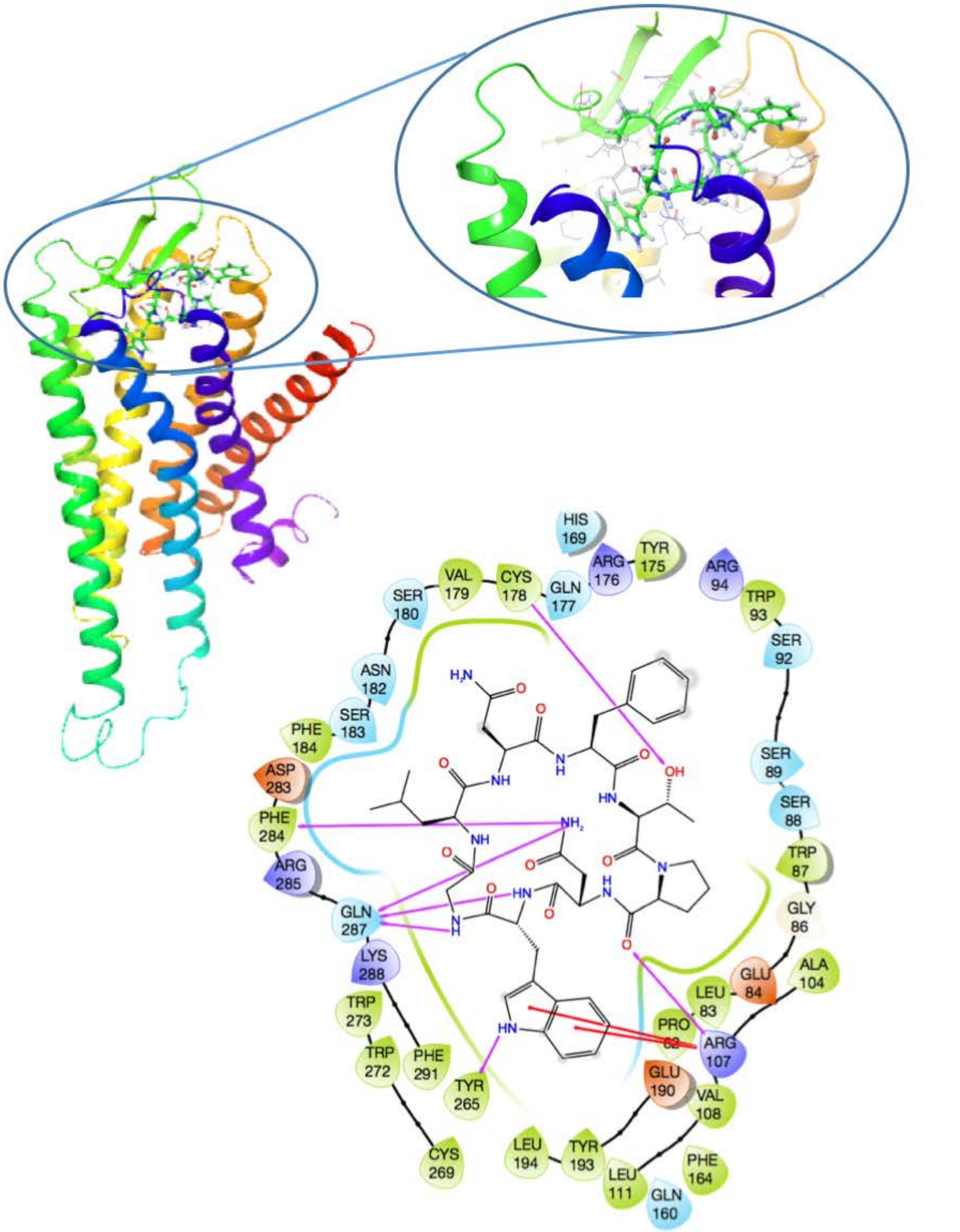
HIS 169
ARG 176
TYR 175
VAL 179
CYS 178
GLN 177
SER 180
ASN 182
SER 183
PHE 184
ASP 283
PHE 284
ARG 285
GLN 287
LYS 288
TRP 273
TRP 272
PHE 291
TYR 265
CYS 269
LEU 194
TYR 193
LEU 111
GLN 160
PHE 164
GLU 190
VAL 108
PRO 82
ARG 107
LEU 83
GLU 84
ALA 104
ARG 94
TRP 93
SER 92
SER 89
SER 88
TRP 87
GLY 86
Charged (negative)
Charged (positive)
Glycine
Hydrophobic
Metal
Polar
Unspecified residue
Water
Hydration site
Hydration site (displaced)
Distance
H-bond
Metal coordination
Pi-Pi stacking
Pi-cation
Salt bridge
Solvent exposure

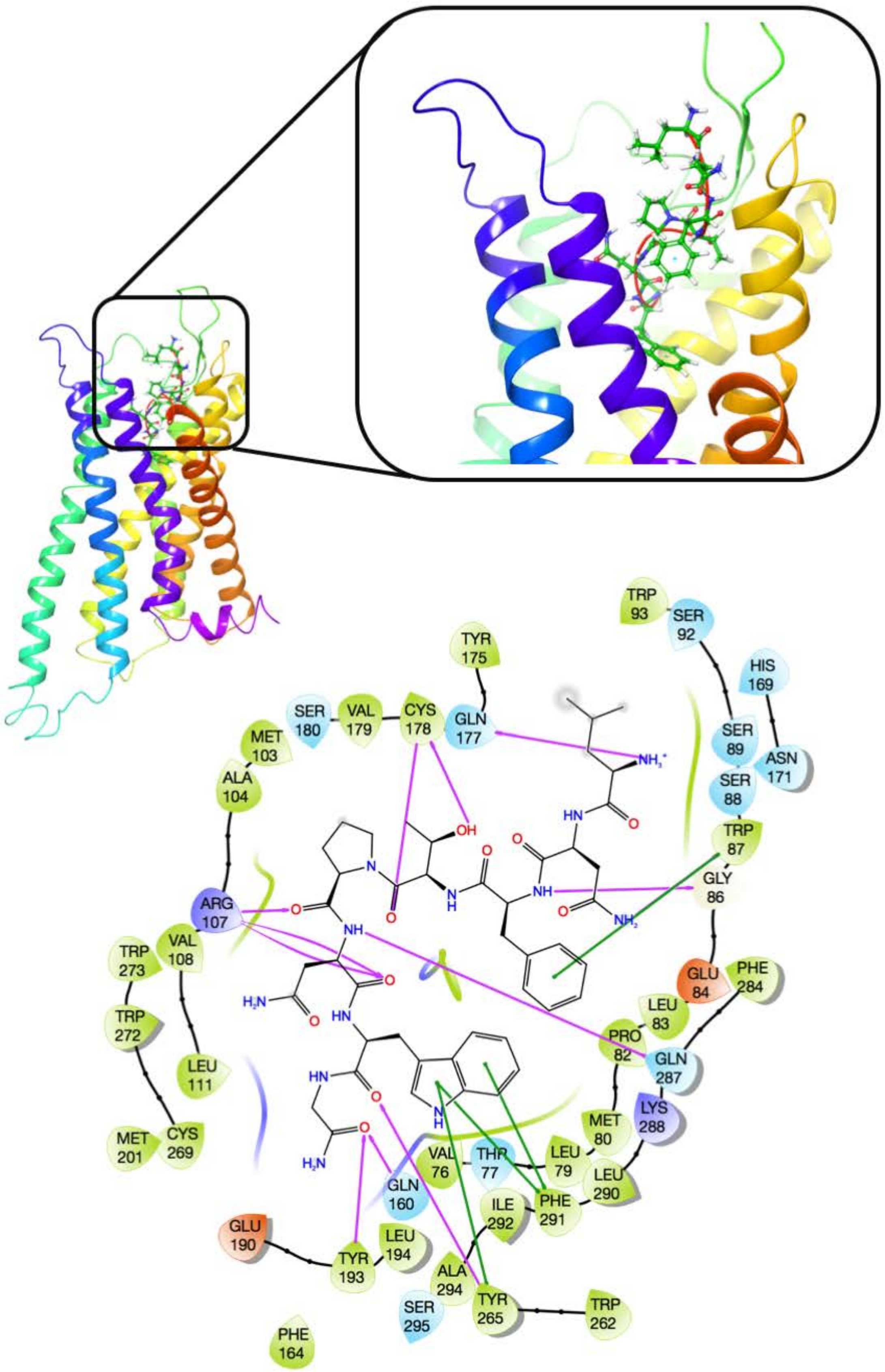
TRP 93
SER 92
HIS 169
TYR 175
SER 180
VAL 179
CYS 178
GLN 177
SER 89
ASN 171
MET 103
ALA 104
SER 88
TRP 87
GLY 86
ARG 107
VAL 108
TRP 273
GLU 84
PHE 284
LEU 83
TRP 272
PRO 82
GLN 287
LEU 111
LYS 288
MET 201
CYS 269
MET 80
VAL 76
THR 77
LEU 79
LEU 290
GLN 160
ILE 292
PHE 291
GLU 190
LEU 194
TYR 193
ALA 294
SER 295
TYR 265
TRP 262
PHE 164

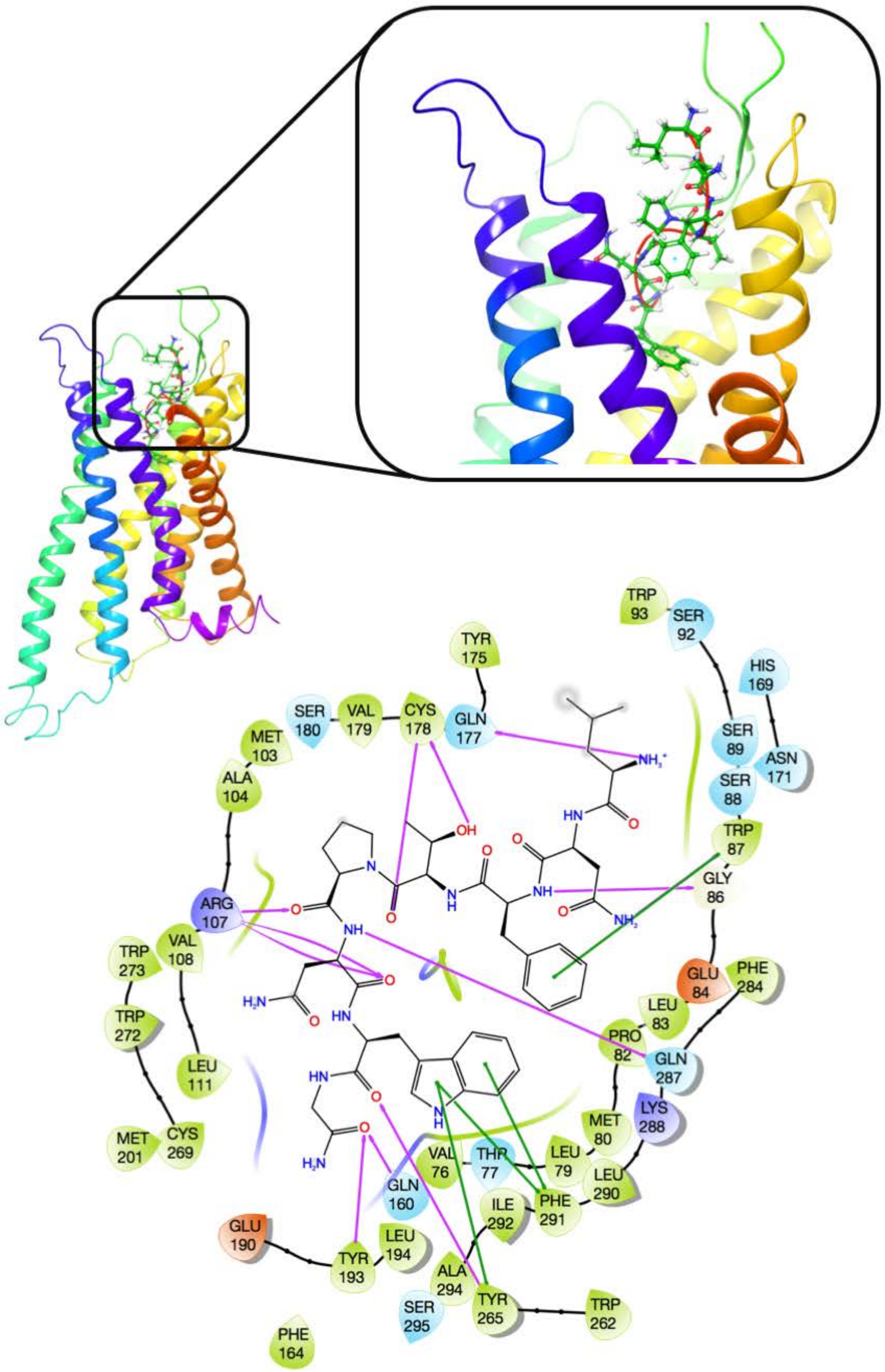
TRP 93
SER 92
HIS 169
TYR 175
SER 180
VAL 179
CYS 178
GLN 177
SER 89
ASN 171
MET 103
ALA 104
SER 88
TRP 87
GLY 86
ARG 107
VAL 108
TRP 273
GLU 84
PHE 284
LEU 83
TRP 272
PRO 82
GLN 287
LEU 111
LYS 288
MET 201
CYS 269
MET 80
VAL 76
THR 77
LEU 79
LEU 290
GLN 160
ILE 292
PHE 291
GLU 190
LEU 194
TYR 193
ALA 294
SER 295
TYR 265
TRP 262
PHE 164

a

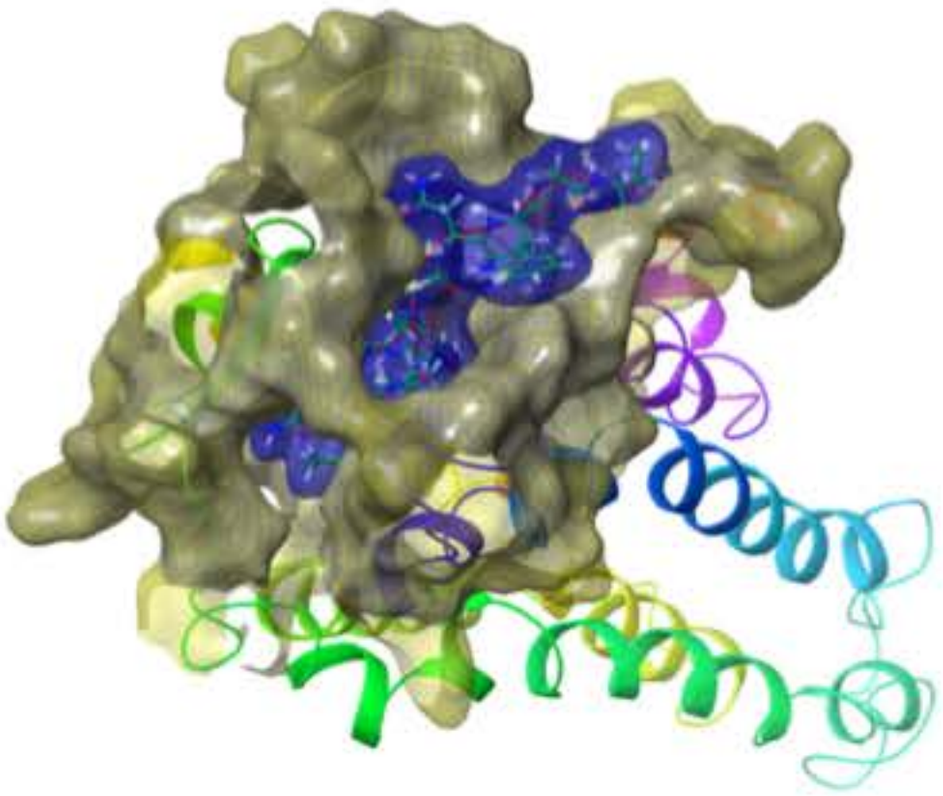

b

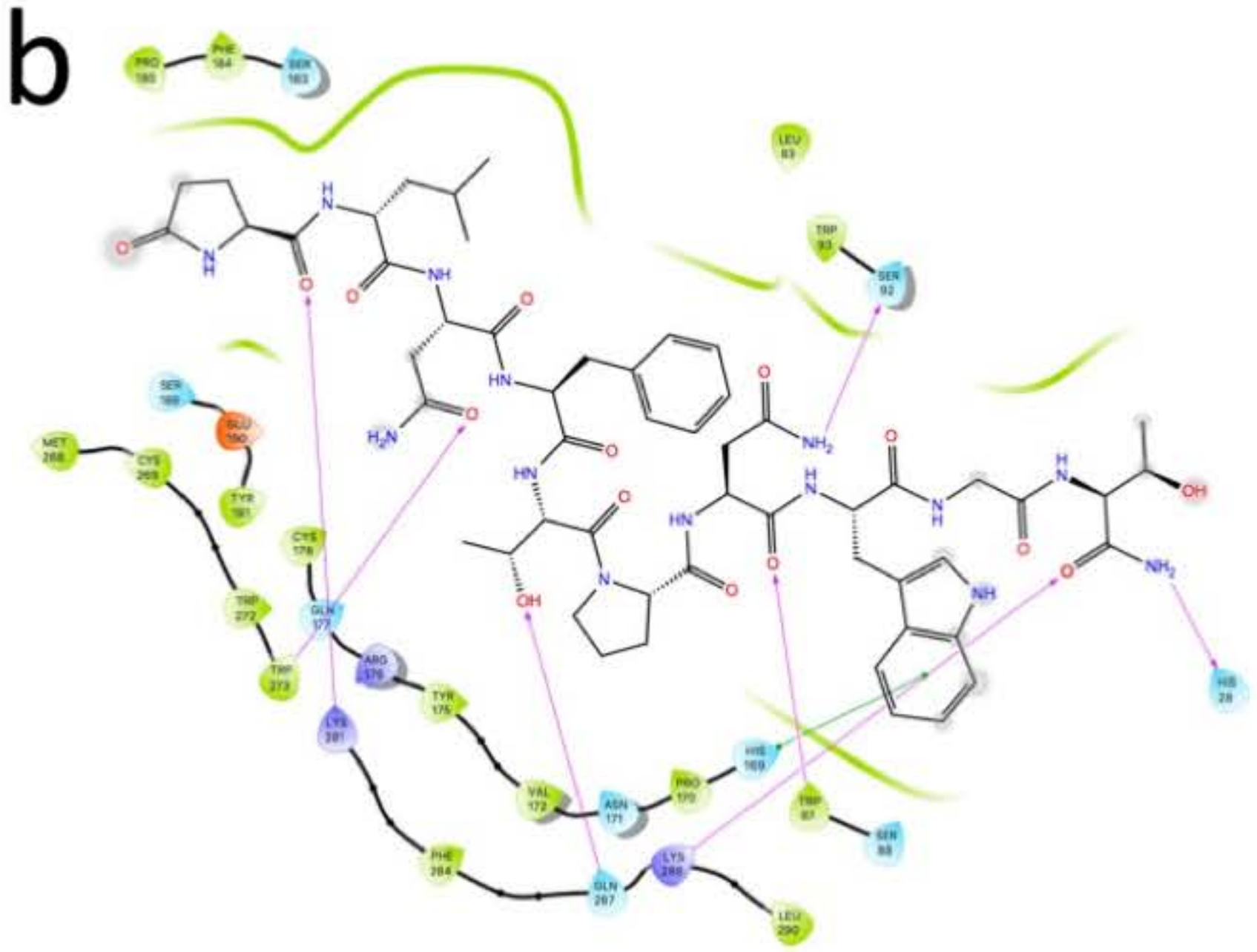
PRO 180
PHE 184
SER 183
LEU 83
TRP 93
SER 92
SER 189
GLU 190
MET 268
CYS 269
TYR 181
CYS 178
TRP 272
GLN 177
TRP 273
ARG 176
TYR 175
LYS 281
VAL 172
ASN 171
PRO 170
HIS 169
TRP 87
SER 88
PHE 284
GLN 287
LYS 288
LEU 290
HIS 28
OH
NH2
NH
HN
NH
N
O

A

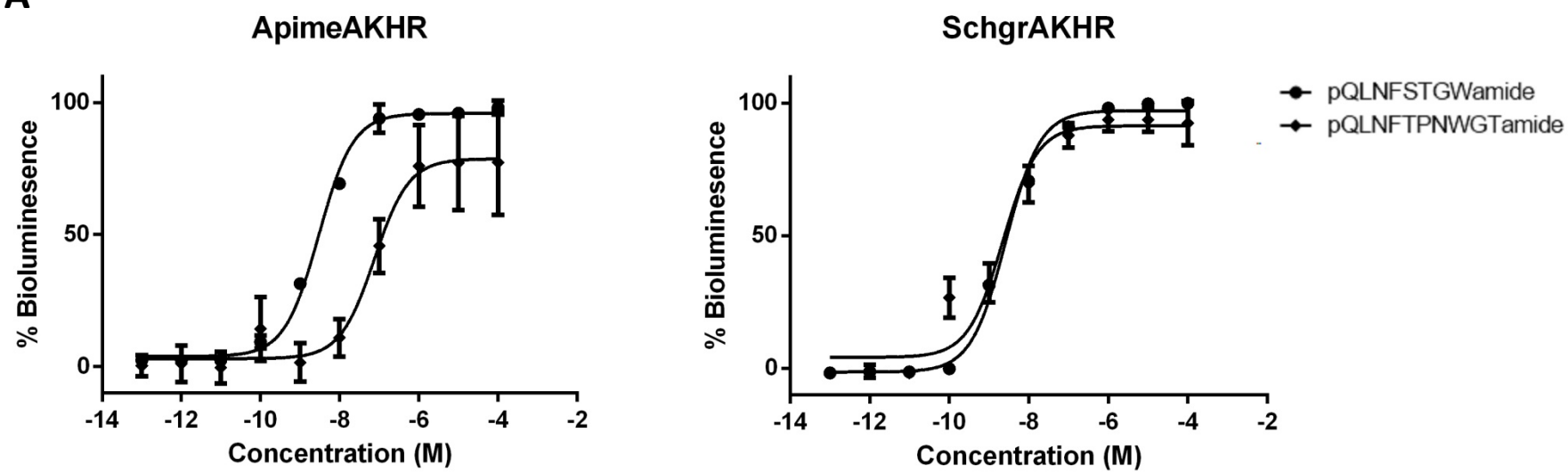
ApimeAKHR
SchgrAKHR
% Bioluminesence
100
50
0
-14
-12
-10
-8
-6
-4
-2
Concentration (M)
pQLNFSTGWamide
pQLNFTPNWGTamide

B

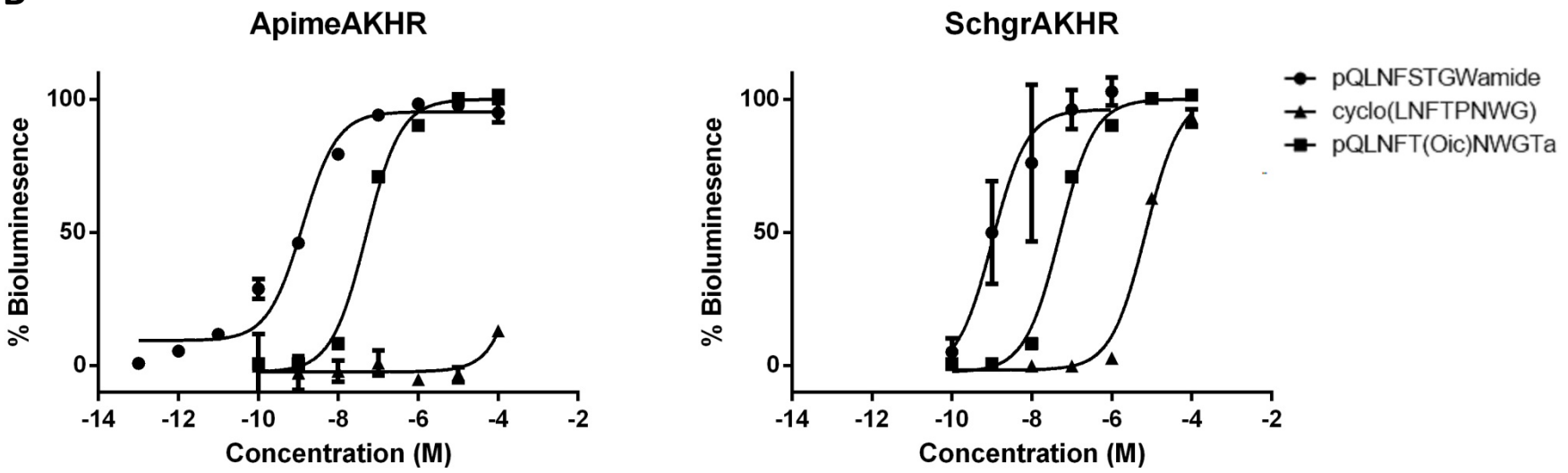
ApimeAKHR
SchgrAKHR
% Bioluminesence
100
50
0
-14
-12
-10
-8
-6
-4
-2
Concentration (M)
pQLNFSTGWamide
cyclo(LNFTPNWG)
pQLNFT(Oic)NWGTa

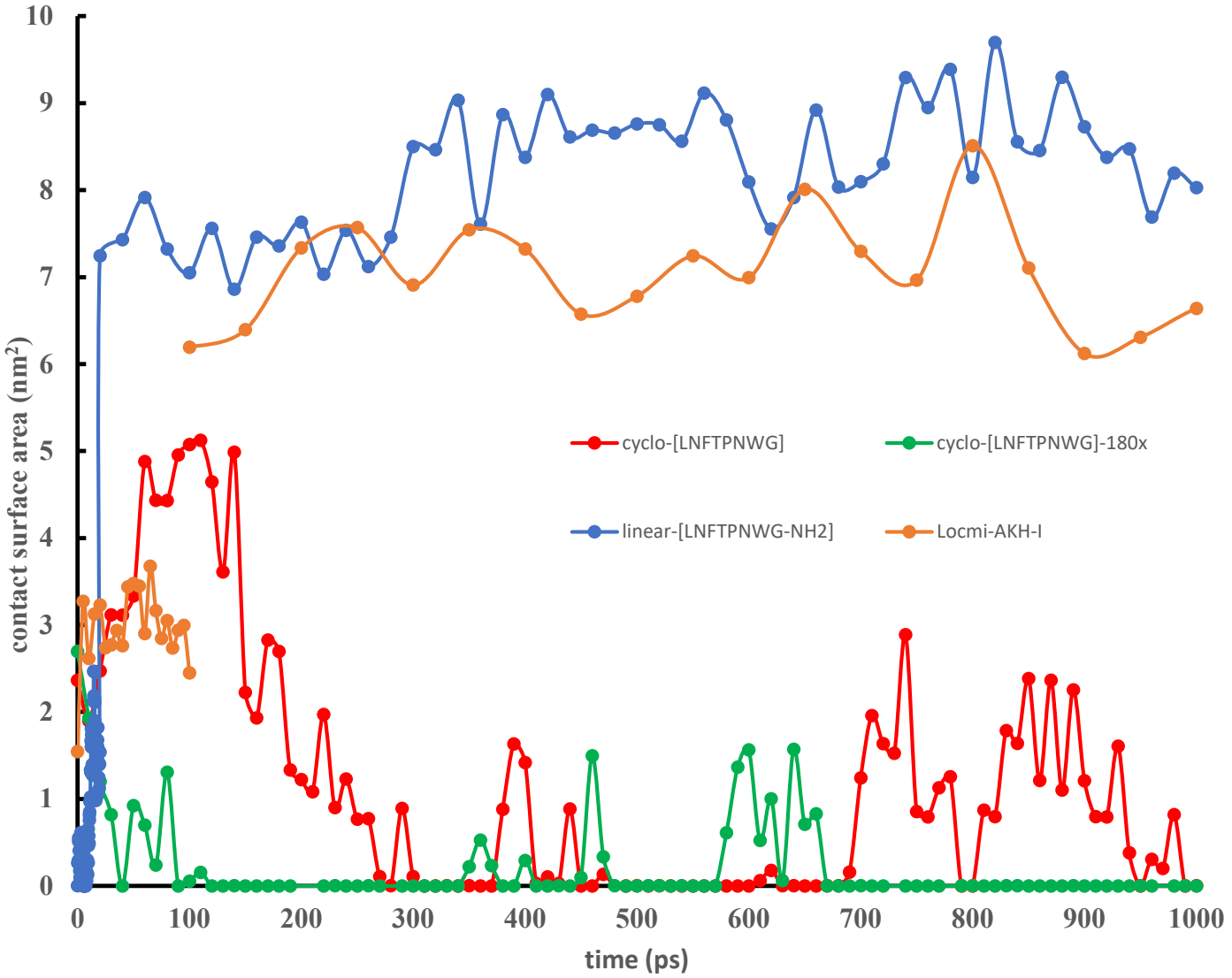
contact surface area (nm²)
time (ps)
cyclo-[LNFTPNWG]
cyclo-[LNFTPNWG]-180x
linear-[LNFTPNWG-NH2]
Locmi-AKH-I
0
1
2
3
4
5
6
7
8
9
10
0
100
200
300
400
500
600
700
800
900
1000

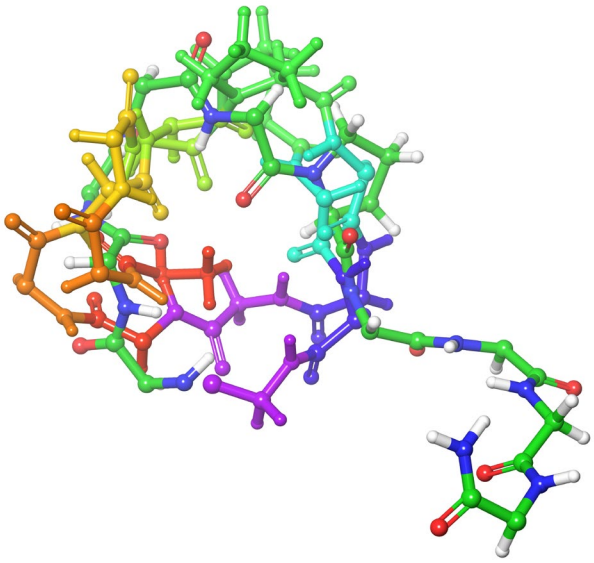

Figure 6. Overlay of cyclo-[LNFTPNWG], linear-[LNFTPNWG-NH2] and Locmi-AKH-I. The cyclo and linear peptide are coloured according to residues position. Locmi-AKH-I is coloured normally.

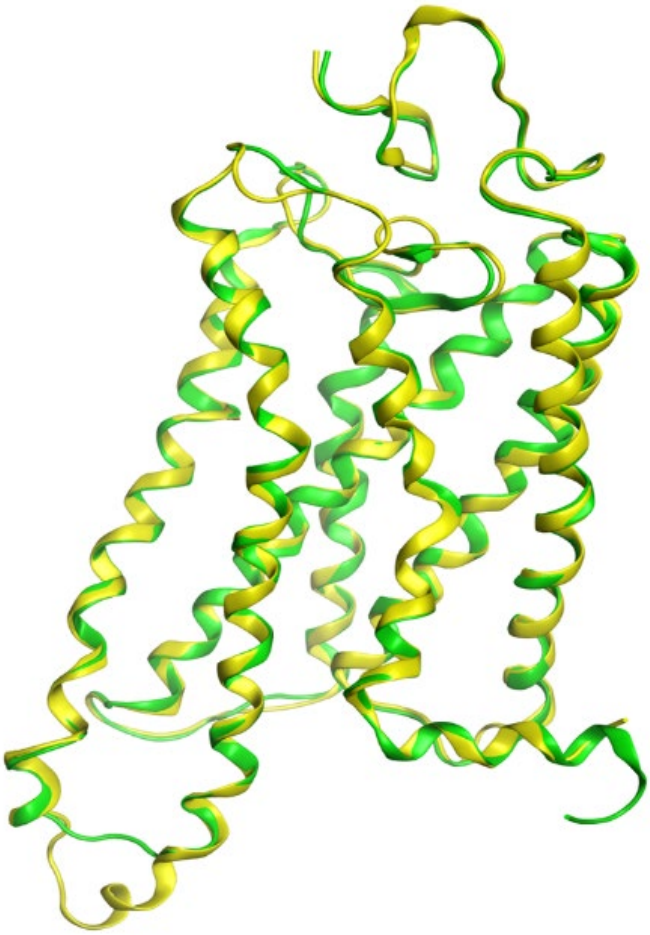

Figure 10. a) An overlay of Apime-AKHR-model (in green) with the apelin receptor (in yellow).

a

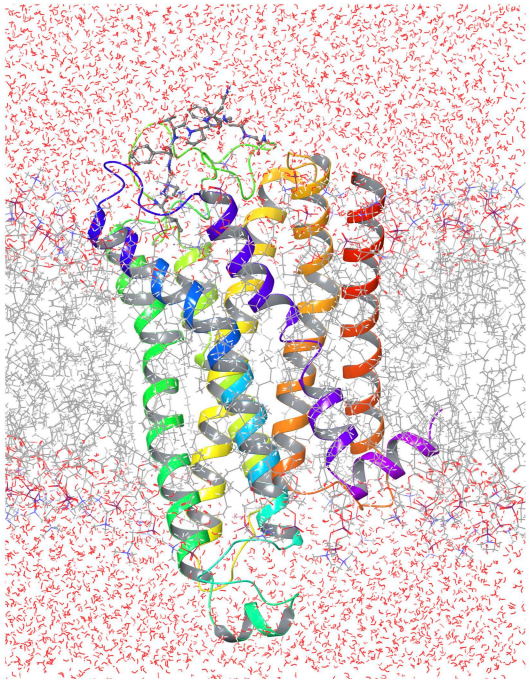

b

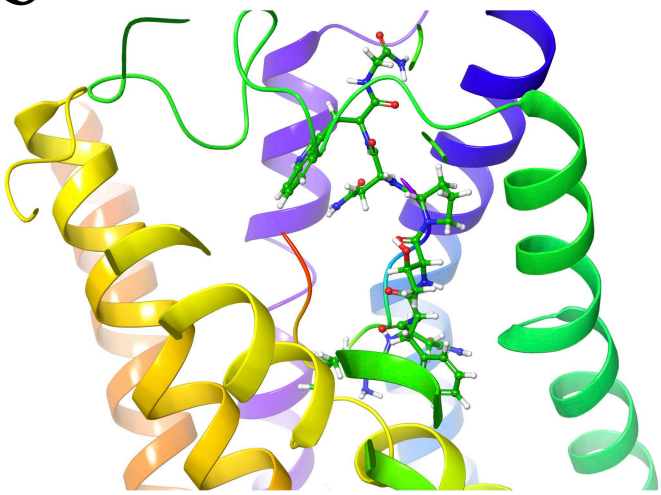

c

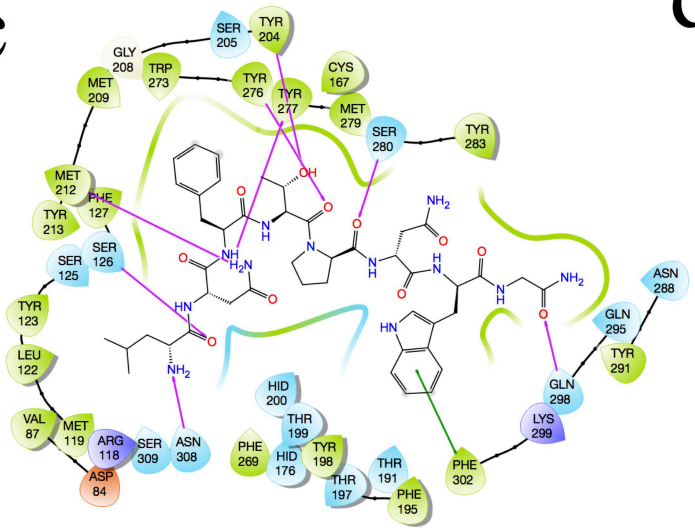
SER 205
TYR 204
GLY 208
TRP 273
MET 209
TYR 276
CYS 167
TYR 277
MET 279
SER 280
TYR 283
MET 212
PHE 127
TYR 213
SER 126
SER 125
TYR 123
LEU 122
VAL 87
MET 119
ARG 118
SER 309
ASN 308
ASP 84
HID 200
THR 199
PHE 269
TYR 198
HID 176
THR 197
THR 191
PHE 195
PHE 302
LYS 299
GLN 298
GLN 295
TYR 291
ASN 288

d

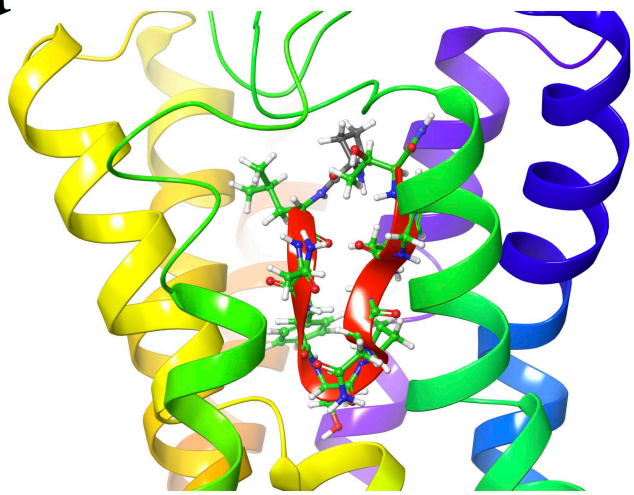

e

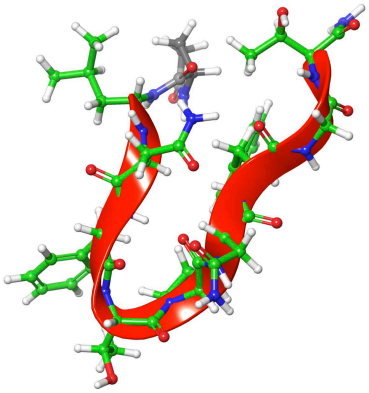

f

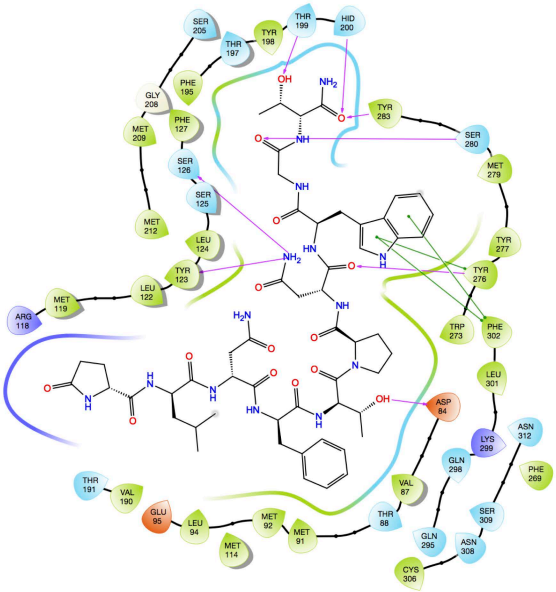
SER 205
THR 199
HID 200
TYR 198
THR 197
GLY 208
PHE 195
PHE 127
MET 209
TYR 283
SER 280
SER 126
MET 279
SER 125
MET 212
LEU 124
TYR 277
TYR 123
TYR 276
LEU 122
MET 119
ARG 118
TRP 273
PHE 302
LEU 301
ASP 84
LYS 299
ASN 312
GLN 298
PHE 269
THR 191
VAL 190
VAL 87
GLU 95
LEU 94
MET 92
THR 88
SER 309
MET 91
GLN 295
ASN 308
MET 114
CYS 306